FEATURE ARTICLE

Advanced Ellipsometric Characterization of Conjugated Polymer Films

Mariano Campoy-Quiles, M. Isabel Alonso, Donal D. C. Bradley, and Lee J. Richter*

Conjugated polymers are attracting worldwide attention due to their potential for use as the active layer in advanced electronic, optoelectronic, and energy harvesting applications, and their cost-effective and low thermal budget processing traits. As the technologies based on these materials develop, new and more sensitive characterization techniques are needed. Recent progress on the use of spectroscopic ellipsometry as a highly sensitive and non-invasive method to obtain fundamental information about conjugated polymer films is reviewed. After a brief introduction to the practical details of the technique, the use of ellipsometry to determine optical parameters that provide insight into film morphology is described, including physical phase and molecular orientation, and resulting electronic structure. The characterization of layered systems and the use of in-situ ellipsometry as a means to gain understanding of the kinetics that occur during film deposition and post-deposition thermal and solvent vapor treatment is also discussed.

1. Introduction

Polymeric semiconductors are an attractive class of optoelectronic materials due to their advantageous traits with respect to cost-effective, low-temperature and high-throughput solution processing coupled with desirable functional characteristics. A myriad of applications, including the use of field effect transistors (FETs),[1] light emitting diodes (LEDs),[2] and photovoltaic (PV)[3] devices for displays, lighting, sensing, and solar energy conversion are under development. In most cases, these materials are deposited as thin film (≈100 nm) layers within a device structure by coating methods such as spin-, dip-, and knife-coating or printing methods such as inkjet-, screen-, and gravure-printing.

As the different technological applications and device architectures develop, new tools for the characterization and optimization of device-layer films are needed. Amongst them, spectroscopic ellipsometry[4–6] is gaining attention as a non-invasive technique that can provide a wealth of useful information. In favorable cases, ellipsometry can provide detailed depth profiles of material composition, physical phase, and molecular orientation in complex multilayer samples. The technique can be applied in-situ and in real-time, allowing both the determination of thin film phase transition temperatures and studies of drying kinetics during film deposition and temporal changes in morphology during post-deposition treatments (thermal and solvent annealing, etc.) Recently, ellipsometry has even been proposed for in-line monitoring of organic photovoltaic (OPV) thin film microstructure during roll-to-roll processing.[7,8]

In this article we set out to provide a focused review of recent advances in the application of ellipsometry to the characterization of conjugated polymer thin films. In the interests of brevity, we do not discuss the many other materials important to the performance of organic optoelectronic devices. These include electrode materials such as Ca,[9] Al,[9] and indium tin oxide (ITO),[10,11] as well as typical flexible substrate materials such as PET and PEN[12] (see Appendix for polymer name abbreviations) and encapsulation films. For the same reason, we do not cover recent work on the optical properties of small molecule (largely in vacuo deposited) semiconductors, such as pentacene,[13] oligothiophene,[14] perylene-3,4,9,10-tetracarboxylic-3,4,9,10-dianhydride,[15] diindenoperylene,[16] tris(8-hydroxyquinoline)aluminium,[17,18] and metal phthalocyanines.[19]

The article is organized as follows. In Section 2, a brief introduction to the measurement and analysis of ellipsometric data of conjugated polymer films is presented; this is specially aimed at newcomers to the field. Emphasis is placed on practical considerations specific to the material complexity inherent to conjugated polymers. Section 3 is devoted to use of ellipsometry to characterize single film layers. Its main emphasis is on the accurate determination and interpretation of the dielectric function and the anisotropy of the dielectric tensor. Section 4 deals with the analysis of more complex vertically structured systems, including multilayer device structures and mixtures of materials, focussing on the description of surface roughness, diffusive (rough) interlayers and bulk heterojunctions. Finally, in Section 5 we review recent results concerning the use of real-time in-situ ellipsometry to characterize thin film phase transitions and to monitor the kinetics of film deposition and post-deposition treatments.

Dr. M. Campoy-Quiles, Dr. M. I. Alonso
Institut de Ciència de Materials de Barcelona (ICMAB-CSIC)
Campus UAB, Bellaterra, 08193, Spain
E-mail: mcampoy@icmab.es
Prof. D. D. C. Bradley
Department of Physics and Centre for Plastic Electronics
Imperial College London
South Kensington Campus, London, SW7 2AZ, UK
Dr. L. J. Richter
National Institute of Standards and Technology
Gaithersburg, MD, 20899, USA

DOI: 10.1002/adfm.201303060

2. From Ellipsometry Data to Material Properties: General Remarks

Ellipsometric measurements allow one to deduce the optical properties of a material based on the changes in the polarization state of light upon reflection from (or transmission through) the sample under consideration. The reflection geometry is more useful in general and particularly for films. In a measurement, the complex reflectance ratio (ρ) of the reflected and incident light polarization states is determined. This ratio is typically presented in terms of the ellipsometric angles Ψ and Δ and for the case of an homogeneous and isotropic material with a flat surface it coincides with the ratio of the complex Fresnel reflection coefficients (r_p and r_s):

$$\rho = \tan\Psi \cdot e^{i\Delta} = \frac{r_p}{r_s} \quad (1)$$

The coefficients r_p and r_s are the diagonal elements of the 2 × 2 Jones matrix appropriate to the description of isotropic systems that lack depolarization. Jones matrices can be used to describe the majority of samples by generalizing the reflection coefficients to deal with multilayers and by taking into account off-diagonal elements for optically anisotropic samples. Only for systems with significant depolarization, it is necessary to consider the full 16 elements of the Mueller matrix, a 4 × 4 generalization of the Jones matrix applied to Stokes vectors.

Ellipsometry, in general, is a ratiometric technique and thus is self-normalized, does not require a reference and is extremely precise. However, it is an indirect technique. The sample parameters of interest: film thicknesses (d) and dielectric functions ($\varepsilon = \varepsilon' + j\varepsilon'' = \tilde{n}^2 = (n + j\kappa)^2$), where n and κ are the real and imaginary parts of the refractive index, $\tilde{n}$, respectively), are obtained by fitting the data to a forward simulation typically via transfer matrix algebra. Like all forward simulation techniques, uniqueness cannot be proven and the accuracy of the results is predicated on the inclusion of all relevant features in the model of the system. Additionally, one must be alert to the numerical and statistical robustness of the analysis: parameters often become highly correlated. A thorough description of the technique can be found in the literature.[4,5,6]

Extracting material properties from spectroscopic ellipsometry data typically involves the following basic steps: 1) preparation of the samples, 2) measuring the ellipsometric angles, 3) analysis of the experimental data via fitting parameters to a forward simulation of the samples, 4) checking the final results for robustness, preferably via correlation with other experimental evidence. In this section, we will briefly discuss these four steps.

2.1. Sample Preparation

The properties of conjugated polymer films depend on the chemical nature of the specific polymer under investigation but, importantly, they also strongly depend on the way in which chain segments are spatially organized in the solid, that is, the polymer microstructure and/or film morphology. In general, polymers reach thermodynamic equilibrium only in the melt state but their solid-state microstructure depends more on kinetic than on thermodynamic factors, exhibiting strong path

Mariano Campoy-Quiles is tenure scientist at ICMAB-CSIC where he leads a group focused on the spectroscopic characterization of fundamental properties and morphology in organic semiconductors and their applications. He obtained a Physics degree from the University of Santiago de Compostela and his PhD in Experimental Physics at Imperial College London. After a fellowship at JAIST in Japan, he moved to ICMAB in 2008.

María Isabel Alonso is a staff research scientist at ICMAB-CSIC. She obtained her BS and MS degrees in Physics from the Autonomous University of Barcelona and her Dr. rer. Nat. from the University of Stuttgart while working at the Max-Planck-Institute for Solid State Research. One of her main research interests is the use and improvement of ellipsometry, in particular to characterize complex materials such as anisotropic and nanostructured samples.

Donal Bradley is the Lee-Lucas Professor of Experimental Physics, Director of the Centre for Plastic Electronics and Vice-Provost for Research at Imperial College London. His research interests span fundamental molecular properties, device physics, materials processing and diverse applications. Bradley also co-invented conjugated polymer electroluminescence, co-founded Cambridge Display Technology and Molecular Vision and is a Director of Solar Press.

Lee J. Richter is a senior scientist in the Material Measurement Science Division at the National Institute of Standards and Technology (NIST). He received his Ph.D. in Physics from Cornell University in 1988 for high resolution and time-resolved vibrational spectroscopy studies of adsorbate bonding and reactivity. His current research is in the development and application of optical spectroscopies, both linear and nonlinear, to the characterization of technologically relevant thin films and interfaces.

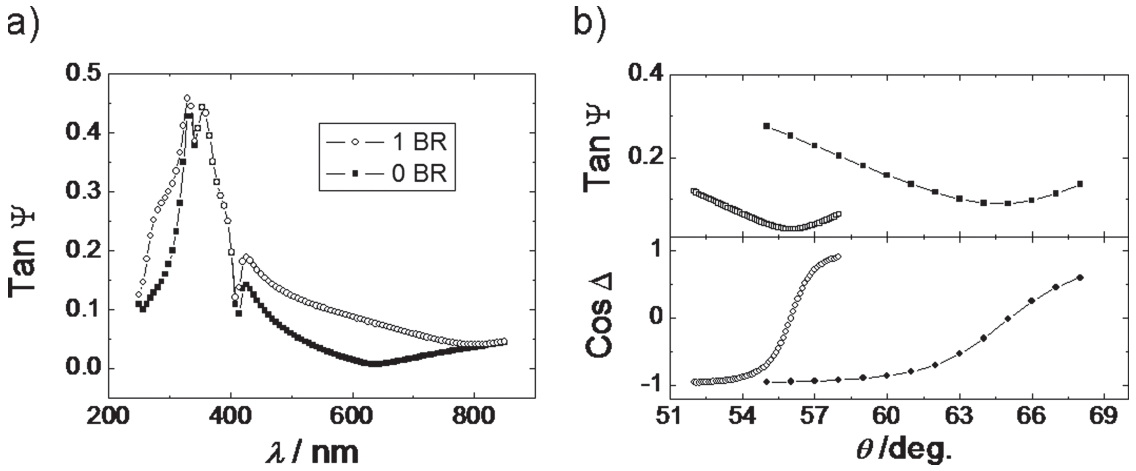

Figure 1. Simulated ellipsometric angles for a 100 nm thick film on a transparent substrate. a) Shows the spectral dependence of tanΨ for PFO when incoherent back reflections at the bottom of the quartz substrate are (empty circles) and are not (filled squares) considered in the simulation. Since, in practice, such incoherent reflections are difficult to model, it is preferable to avoid this additional complication. b) Shows the predicted ellipsometric angles tanΨ (squares) and cosΔ (circles) at 550 nm as a function of incidence angle for PMMA (open) and PFO (filled symbols). At the effective Brewster angle the value of tanΨ is minimum and cosΔ is close to zero (i.e., the polarization variation is large).

dependence in terms of processing. The optical properties are thus a function of both chemical nature and processing. In the case of conjugated polymers, it has been found that, besides the specific chemical structure, n and κ can depend on molecular weight,[20,21] deposition method,[22–24] solution concentration, film thickness,[22,24,25] and so on, or at least indirectly so, through the changes in microstructure that arise. Moreover, we have often noticed that the microstructure and concomitantly the deduced optical properties depend on the substrate upon which the film is deposited. For instance, for a given solution, spin coated films on silicon wafers are often thinner and exhibit a different degree of anisotropy than corresponding films on glass. Surface roughness and surface energy of the substrate will influence the deposition of the organic film; these and other issues will be discussed in more detail in the following sections. The lack of standardized material synthesis routes and film-processing protocols requires that a clear delineation of material and substrate characteristics and processing methods should be provided in order to ensure reproducibility.

2.2. Measurement Considerations

The optical properties of conjugated polymers are often quite complex, exhibiting several asymmetric absorption bands and shoulders in their visible range spectra. These comprise different (predominantly π-electron based) electronic transitions and their vibronic replicas.[27] The vibrational quanta coupled to the electronic states are associated with relatively high frequency vibrations; carbon–carbon stretching and bending in the most part, but also carbon-heteroatom (N, S, O, etc.) modes. This results in large transition bandwidths with, depending on the degree of order, more or less well-resolved vibronic peaks.[28,29] For simplicity, these vibronically structured peaks are normally modelled in ellipsometry as single asymmetrically broadened electronic transitions.[30] The particular molecular conformation, the existence of mono-/multi-domain orientation and the coexistence of different microstructures gives rise to further complications. Lateral and vertical variations in composition, conformation or state of order need also to be considered. Therefore, in order to extract reliable information from the ellipsometric data, it is important to optimize the sample and measurement conditions. In terms of the samples, the film thickness should be typically greater than 20–30 nm in order to allow decorrelation of the optical properties and film thickness.[4] Large surface roughness or density variations within the film should also be avoided. The use of a weakly focused beam (spot sizes between 100 μm and 300 μm) is often beneficial in removing the effect of large-scale film inhomogeneities; nanoscale heterogeneity, however, offers substantial challenges to the extraction of information beyond a global average. The choice of substrate is also important; generally, higher index contrast (such as that provided by films on silicon rather than on glass) enhances the signal to noise ratio of the experimental data.[30] When using transparent substrates, it is important to try to avoid incoherent reflections at the bottom of the substrate, as they will strongly affect the measurement (see **Figure 1**a) and are not easily controlled. However, as already mentioned, the substrate may also alter the properties of conjugated polymer layers; direct measurements on device structures or at least on device substrates may then be important to an understanding of layer function.

As for the measurement itself, variable angle spectroscopic ellipsometry (VASE) is the preferred, although not always sufficient experiment. The angles of incidence should include values around the effective Brewster angle of the sample, where the largest changes in polarization occur and the ellipsometric measurements are most sensitive (Figure 1b).[31] Spectroscopic experiments are needed to determine the dispersion of optical constants and single wavelength experiments should be generally avoided other than to determine film thickness for well-known (fully characterized) materials. However, in order to extract reliable information for such complex systems

as conjugated polymer films, one typically requires greater data diversity than is available from a simple VASE study. A number of experimental protocols have been proposed that include: 1) combined VASE and optical transmission measurements,[32,33] 2) multiple sample analysis with varying thin film thickness,[34] 3) multiple sample analysis with fixed film thickness but varying the substrate,[35] and 4) interference enhancement VASE.[30]

It is important to emphasize that given the strong connection between processing conditions and resulting optical properties, multisample analysis via substrate diversity (for instance, using substrates consisting of silicon wafers with thermally grown oxide layers of different thickness) at fixed film thickness is to be preferred over variation in film thickness.

2.3. Analysis of the Data

Extracting material properties such as refractive index, absorption (extinction) coefficient and film thickness from VASE data requires building mathematical models to describe the sample(s) under consideration. This is, probably, the most challenging part in any ellipsometric experiment. As stated earlier, in general a set of ellipsometry data, that is, spectra acquired at multiple angles on possibly multiple samples (varying film thickness and or substrate), are fitted to a forward simulation based on a physical model. The fit is adjusted to minimize a figure-of-merit, FOM, that is typically the reduced root, χ^2:

$$\mathrm{FOM} = \sqrt{\frac{1}{2N-m}\sum_{j=1}^{N}\frac{\left(\Psi_j^{\exp t}-\Psi_j^{\exp t}\right)^2}{\sigma\Psi_j^2}+\frac{\left(\Delta_j^{\exp t}-\Delta_j^{\exp t}\right)^2}{\sigma\Delta_j^2}} \quad (2)$$

where N is the total number of Ψ–Δ pairs (wavelength, angle-of-incidence, substrate), m the number of model parameters, and σ the point-wise experimental errors. For a typical VASE multi-sample analysis, N can be of order 6000 and m, for a wavelength-by-wavelength model (see below), can be in excess of 1000. There is significant variation in the literature (and across vendors) in the adopted FOM. Both weighted and unweighted forms are used; additionally, the square error can be computed based on Ψ and Δ, $\tan\Psi$, and $\cos\Delta$, Re[ρ] and Im[ρ], or the Mueller matrix related parameters: N, C, and S.[4–6] Proper statistical interpretation of the complex minimization problem is beyond the scope of this paper. In general, it is best to fit parameters that are natural, that is, exhibit the assumed stochastic variance ($\tan\Psi$ and $\cos\Delta$ or N, C, and S). For statistical interpretation of errors, weighting is required. As the system is highly nonlinear and the distribution of errors is often unknown, both Monte Carlo and bootstrap methods can be usefully applied.[36]

The models used in ellipsometric data analysis are based on two basic sets of physical parameters: those that describe the vertical structure (film thickness, interphase thickness and composition, surface roughness, etc.) which are simulated by a stack of layers and those that describe the dielectric function (the anisotropy and wavelength, λ, dependence of $\varepsilon[\lambda]$) For the simplest case of a semi-infinite, isotropic substrate with a flat, abrupt interface with a known ambient (typically vacuum or air), the two observables Ψ and Δ at each wavelength can be analytically inverted to obtain n and κ versus λ.[4] Thus ellipsometry is routinely used to obtain quality reference dielectric functions for materials. In most other cases the structural parameters and the dielectric functions are obtained using numerical inversion. An important constraint on $\varepsilon[\lambda]$ is that it must be causal and obey the Kramers-Kronig (KK) relations. Typically, the obtained dielectric function data, even from analytical inversion, is tested against the KK relations to confirm consistency.

Unfortunately, due to the frequently strong variation in the microstructure of conjugated polymers with processing, the optical properties deduced for thicker layers are rarely a good guide to those for technologically relevant thin films. The film spectrum must then be interpreted by considering a multilayer model that includes both the structural and the optical unknowns. However, most conjugated polymer films exhibit two distinct regions within the spectral range accessible for commercially available ellipsometers, a higher energy region where most absorption transitions occur, and a lower energy transparent region towards the IR. Given the typically high absorption coefficients of conjugated polymers at their peak maxima ($\alpha \approx 10^5$ cm^{-1}), light with corresponding wavelengths only propagates a few tens of nm before it is strongly attenuated. Therefore, it may be helpful to obtain a very crude estimate of the shape and magnitude of the absorption using analytical inversion. It should also be mentioned that conjugated polymer films are often anisotropic. The determination of the different dielectric function components needed to describe an optically anisotropic system therefore requires measurements at several angles of incidence and/or several in-plane azimuths.[37] A common difficulty arises from the fact that the ellipsometric measurement is dominated by the in-plane dielectric function contributions $\varepsilon_{\parallel}$ and determination of $\varepsilon_{\perp}$ is rather difficult on bulk samples.[38,39]

The majority of ellipsometric studies are made on systems comprising a thin conjugated polymer film on top of a known substrate such as glass, quartz, SiO_2 coated Si, glass/ITO/PEDOT:PSS (a typical polymer diode bottom anode contact), or gold. In this geometry, two main data analysis approaches are commonly used to obtain the optical properties of the thin film: i) wavelength-by-wavelength (λ-by-λ) numerical fits and ii) parametric description of the dielectric function.[4–6]

Direct λ-by-λ fits are extremely useful as no multipeak modelling is required and thus very complex absorption profiles can be reproduced. If the data set contains sufficient diversity, the full set of parameters: ni [λ], κi [λ] and d_i, where i is the layer index, can be obtained. Such a fit is numerically intensive and problematic with respect to issues of correlations and local minima. In this approach, previous knowledge of the film thickness, provided by complementary techniques, such as profilometry or atomic force microscopy (AFM), or even by a simple analysis of the transparent region of the VASE data (assuming $\kappa = 0$) can be critical in finding the proper global minimum prior to a full fit. In general this approach is very sensitive to noise and systematic errors in the data. Thus a simultaneous fit for several samples (multisample analysis) may help the convergence into a physical description of the dielectric function. The validity of the numerical fitting can be tested against KK relations as with direct inversion. Recently the introduction of KK-consistent smooth functions described

by a number of nodes (such as splines) has been used to extract the n and κ of carbon-based materials.[40] This is a powerful approach that assures causal results and improves the convergence and smoothness of the resulting values with respect to a λ-by-λ analysis.

The other approach to extract optical properties of materials from ellipsometric data consists in using parametric models for the dispersion relations of $n(\lambda)$ and $\kappa(\lambda)$. In this case, the dependence of the optical constants on the wavelength of light is described by a mathematical model, such as a Cauchy law or a series of Lorentzian peaks.[5] For instance, Equation 3 shows the Cauchy law, which often is used for transparent materials, where A, B, and C are three fitting parameters varied during the regression:

$$n = A + \frac{B}{\lambda^2} + \frac{C}{\lambda^4} \tag{3}$$

The principal disadvantage of parametric models is a loss of flexibility in the description of the dielectric function. Only features assumed to be present by the choice of model will be represented in the fit. They do, however, have a number of advantages: i) the functions can be chosen to be KK consistent, ii) an appropriately chosen dielectric function can be correlated to fundamental electronic properties such as the energy band structure of inorganic semiconductors,[41,42] or the plasma energy/conductivity of metals,[43] iii) an analytical expression of the optical constants is then available for use in other models and can be parameterized for descriptions of alloys, and iv) for a number, L, of spectral points (typically between 100 and 500), the parametric model tranforms the fitting process from $2L$ unknowns in a point-by-point calculation, to a smaller number, P, of unknowns that typically varies between ≈3 and ≈10–30 for transparent and absorbing materials, respectively. This reduction in fit parameters facilitates a more robust convergence.

Several parametric models for the dielectric function have been employed in the context of conjugated polymers and will be discussed in Section 3 below in relation to the physical nature of the electronic excitations in these materials.

2.4. Complementary Techniques

To verify ellipsometrically deduced values, the structural data should be contrasted with results from alternative techniques. Typically, the thickness of a polymeric film can be readily estimated using profilometry or AFM. X-ray reflectivity has also recently been used as a powerful check on thickness and density.[44] The absorption coefficient (α) obtained from transmission data can be used to double check the ellipsometrically deduced extinction coefficient ($\alpha = 4\pi\kappa/\lambda$)[45] or, in combination with the VASE data, directly inserted in the fitting procedure.[32]

3. Characterization of Single Layer Films

3.1. Optical Spectrum and Electronic Transitions

The spectrum of singlet electronic transitions in conjugated polymer films critically affects their use in devices that rely on photon absorption (photodetectors and solar cells) and emission (LEDs, lasers and optical amplifiers) across the UV through visible to near infrared region. The molecular nature of these polymeric systems (strong intramolecular bonding but relatively weak, often van der Waals, intermolecular bonding) leads to a relatively large localization of the electronic wavefunctions, further enhanced by twists, bends and other conjugation length limiting disorder. This contrasts with Bloch states in inorganic semiconductors that delocalise over the entire crystal. Combined with an intrinsically low dielectric function (≈3 in the transparency region) resulting from the low-Z of the atoms typically present in the polymer chain (predominantly C and H with in many cases a fraction of N, S, and O atoms) and a reduced solid-state packing density, this generally leads to strongly bound electron-hole pairs, that is, excitons as the primary photoexcitations.[27,46] Compared to their inorganic semiconductor counterparts for which excitons are typically weakly bound and can dissociate at room temperature, excitons in conjugated polymers normally have large binding energies (≈0.3–0.5 eV).[27,47] In the absence of significant charge transfer character the oscillator strengths are correspondingly large, giving rise to strong absorption coefficients and large radiative transition rates. Furthermore, these materials display strong electron-local vibrational mode interactions, and as a consequence, transition lineshapes are determined by a Poisson distribution of the oscillator strength over a series of vibronic sidebands, characterized by a Huang-Rhys parameter corresponding to the average number of vibrational quanta coupled to the electronic transition.[28,29] The visibility of the vibronic peaks depends strongly on the degree of disorder present in the film; inhomogeneous broadening reduces visibility. Charge-transfer character can be molecularly engineered by incorporation of moieties that localise the occupied and unoccupied molecular orbitals at different spatial locations in the chain.[48,49] This results in reduced oscillator strength (due to a reduced spatial overlap of initial and final state wavefunctions) and red-shifted absorption and emission transitions with consequently longer radiative lifetimes. These charge transfer transitions have a greater sensitivity to dielectric environment induced chromatic shifts and typically show little vibronic structure. A single material may display both charge transfer and neutral exciton transitions.

There have been several attempts to systematically compare how well different dispersion laws fit ellipsometry data for thin conjugated polymer and macrocycle films. Arwin and Jansson[50] compared Lorentzian (harmonic oscillator analysis, HOA), Gaussian, relaxed-Lorentzian (equivalent to excitons) and critical point lineshapes for polythiophene films. Liu et al. carried out an equivalent study for metal phthalocyanines.[51] Quantum mechanics based models such as Adachi's model dielectric function (MDF),[5,52] standard critical point model (SCP),[5,39] and the Forouhi-Bloomer model[53] (FB) have also been used for the description of different polyfluorene thin films.[30,54,55]

Interestingly, the conclusion of the above investigations is similar: asymmetric peaks (such as asymmetric Lorentzians) are the most suited lineshapes to describe the optical properties of conjugated polymers. This lineshape arises from electron-local

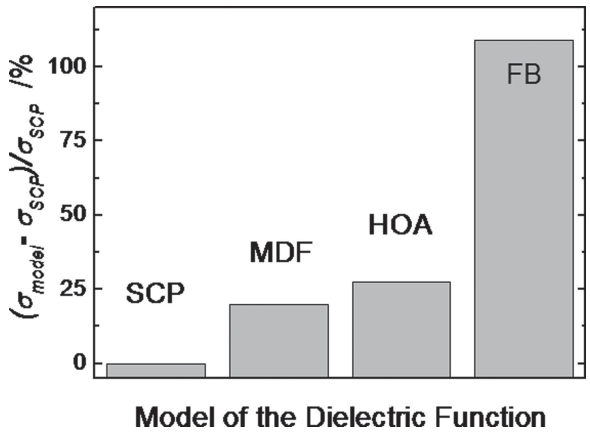

Figure 2. Comparison of the statistical standard deviation (weighted χ^2 representation derived from SOPRALAB software) for fits of the variable angle ellipsometric data for a 98 nm thick PFO film on quartz using the standard critical point (SCP), Adachi's model dielectric function (MDF), the harmonic oscillator analysis (HOA) and the Forouhi-Bloomer (FB) models.

vibrational mode interactions subjected to inhomogeneous broadening.[56] The phase added to a conventional Lorentzian peak is a phenomenological approximation to vibrational effects which allows for energy asymmetric electronic transitions.[41,54] This excitonic model has been successfully applied to many polyfluorenes[30,54,55] and polythiophenes,[50,54,57] and also to macrocyclic phthalocyanines,[51] and molecular crystals.[15] As an example, **Figure 2** shows the normalized standard deviation for the fit of the ellipsometric data for a thin poly(9,9-dioctylfluorene) (PFO) film using four models for the dielectric function. The excitonic model is, on the one hand, the one that best fits the experimental data, and on the other hand, most consistent with the anticipated underlying physics.

It has been pointed out that the electronic wavefunction of highly crystalline organic materials, such as regioregular P3HT, might be more delocalized in up to two dimensions,[58] as compared to the full spatial localization represented by Frenkel excitons. For these cases, a more general model is needed. The standard critical point model developed by Cardona and co-workers[41,56] is one of the possible available models for this purpose.[5] Critical points of 3D, 2D, 1D, and 0D (excitons) are described with a general analytical lineshape:

$$\varepsilon(E) = UV_{\text{term}} - \sum_{j=1}^{M} [A_j e^{i\phi_j} (E - E_{cj} + i\Gamma_j)^D] \quad (4)$$

Where $\varepsilon(E)$ is the dielectric constant as a function of energy (E), which consists of M critical points whose dimension is given by D, and are characterized by amplitude A_j, critical point energy E_{cj}, broadening Γ_j and phase ϕ_j. In this representation, an exciton is obtained for $D = -1$. The electron-local vibrational mode interaction is considered by including the excitonic phase ϕ_j for each transition. This model has been recently employed in the context of organic semiconductors with the aim of accounting for different degrees of electron localization.[54] The treatment of the ellipsometric data using the SCP model allows one to distinguish between localized excitons for amorphous polymeric films, and 1D/2D delocalization of the electronic wavefunction for films containing chains with planar conformations or for highly crystalline films.[54]

A description based on a 1D density of states has also been employed by Zhokhavets and co-workers in order to estimate the exciton binding energy (E_b) from the dielectric function of polythiophenes.[59] Here, the band edge is compared to a modelled 1D band gap in order to extract E_b. This approach yields E_b values of around 0.6 eV for P3OT[59] and for PFO,[60] in reasonable agreement with E_b values obtained with other techniques.[47]

A comparison between a multi-oscillator (Lorentz) description of the ellipsometrically deduced dielectric function of two low band gap polymers and density functional theory calculations has revealed qualitative agreement but some quantitative discrepancies in respect of the transition energy positions.[61] More studies in this direction would, without doubt, provide further insights into the light-matter interactions and electronic transitions in conjugated polymers.[62]

An alternative, more natural description of the excitations in conjugated polymers, as discussed above, is in terms of weakly coupled molecular transitions with strong, local, vibronic coupling. The simplest model that captures this is the Huang-Rhys description that, in appropriate limits, produces asymmetric aggregate lineshapes similar to the SCP models. This has been successfully applied to the spectra of P3HT by multiple groups.[63,64] In both transmission spectroscopy[65] and ellipsometry[63] it has been noted, however, that the simple Huang-Rhys description does not appear to fully describe the evolution of the spectrum with local order. Recently, an alternative theory has been developed for polymer systems based on weakly coupled H-aggregates.[66] It allows extraction of an interchain band-width and intra-chain order (conjugation length) from the polymer absorbance.[67,124]

3.2. Molecular Preferential Orientation and Optical Anisotropy

As already mentioned, the optical anisotropy depends both on the intrinsic anisotropic properties of polymer chains and it also reflects the material microstructure. Conjugated polymers often exhibit rigid-rod-like orientation behavior. This can give rise to thermotropic liquid crystallinity as is prevalent in polyfluorene homopolymers and copolymers.[68,69] Monodomain orientation is then possible using rubbed polyimide and other alignment layers, offering the prospect of polarized light emitting diodes that are of potential interest for backlighting liquid crystal displays.[70,71] In addition, even when thin (≈100 nm) films are simply spin-coated from solution, the incorporated polymer chains can preferentially align with their axis parallel to the plane of the substrate. Because the chain backbone directions are randomly distributed on the film plane, such molecular ordering results in polymeric films that exhibit uniaxial optical behavior with the unique optic axis perpendicular to the plane of the substrate.[72,73]

That is, the out-of-plane direction is optically described by the extraordinary refractive index (n_e) and the in-plane direction by the ordinary one (n_o). In these films the magnitude of the

birefringence $|n_e - n_o|$ and its sign depends on the internal orientation of the mean transition dipole relative to the chain axis. The largest possible anisotropies are obtained when the angle β subtended between the polymer axis and the transition dipole takes values around 0 and 90 degrees, whereas $\beta \approx 55°$ (magic angle) gives an optically isotropic film.[30] In the most common case $\beta \leq 55°$, that is, the dipole moment is rather parallel to the polymer chain giving $n_o > n_e$. This holds for many semiconducting polymers, including polyacetylene,[74] and derivatives of poly(p-phenylene),[75] poly(p-phenylenevinylene),[76–78] polyarylenephenylene,[79] polyfluorene[54,80] and polythiophene.[22,25,34] However, for some cases such as blue emitting PVK, the transition dipole moment is roughly perpendicular to the chain direction, which leads to the extraordinary index being larger than the ordinary.[72,73,81] Another factor to be considered is the axial symmetry or rotation about the chain axis, which tends to reduce the birefringence except in the case $\beta \approx 0°$.

For most conjugated polymers, values for $|n_e - n_o|$ in the transparency region of the spectrum vary between 0.1 and 0.3. However, the dominant influence on the measured anisotropy is the degree of molecular ordering. Ramsdale and Greenham,[9] for instance, showed that while films of materials such as PFB and TFB that have little tendency to order, display weak birefringence, those of materials that characteristically tend to align more easily, such as liquid crystalline F8BT, exhibit larger anisotropies (see **Figure 3**). This is consistent with a recent report that the degree of anisotropy in polythiophene films strongly depends on the regioregularity of the material, and increases with crystallinity.[82] It is also consistent with the higher anisotropies which can be found for aligned liquid crystalline films.[30,81,83–85] For uniaxially oriented monodomain liquid crystal samples the refractive index is substantially enhanced along the chain orientation axis allowing design of microcavity structures with spectrally separated and highly polarized emission components[86] and optimization of optical gain properties.[87,88] Combined measurements of Raman anisotropy and optical dichroism allow extraction of the liquid crystalline order parameter and optical transition dipole moment angle relative to the extended chain axis.[30,89,90] In-plane chain alignment usually gives films with optically uniaxial anisotropy such that, unlike spin-coated films, the unique optic axis is on the film surface. This uniaxial behavior is a result of the incomplete alignment and also of the distribution of chains rotated about their axes. In some cases with improved alignment (or if $\beta \approx 0°$) the observed anisotropy may be biaxial.

A proper description of the anisotropy is critical for accurate ellipsometric analysis. Neglecting anisotropy will introduce systematic errors in film thickness and in the dispersion of the dielectric function. Additionally, quantitative analysis of the anisotropy can provide significant insights into film morphology. This is particularly important to the study of thin film transistors, where the anisotropy in the transport properties results in strong correlations between film orientational order and performance. [83–85] Film anisotropy is also critical to the understanding of OLEDs,[80] particularly outcoupling efficiency,[85] lasers[87,91] and will be important in the characterization of the angle-of-incidence dependence of OPV devices.

Fundamentally the film morphology is a function of both thermodynamics and kinetics. It is not surprising then that the

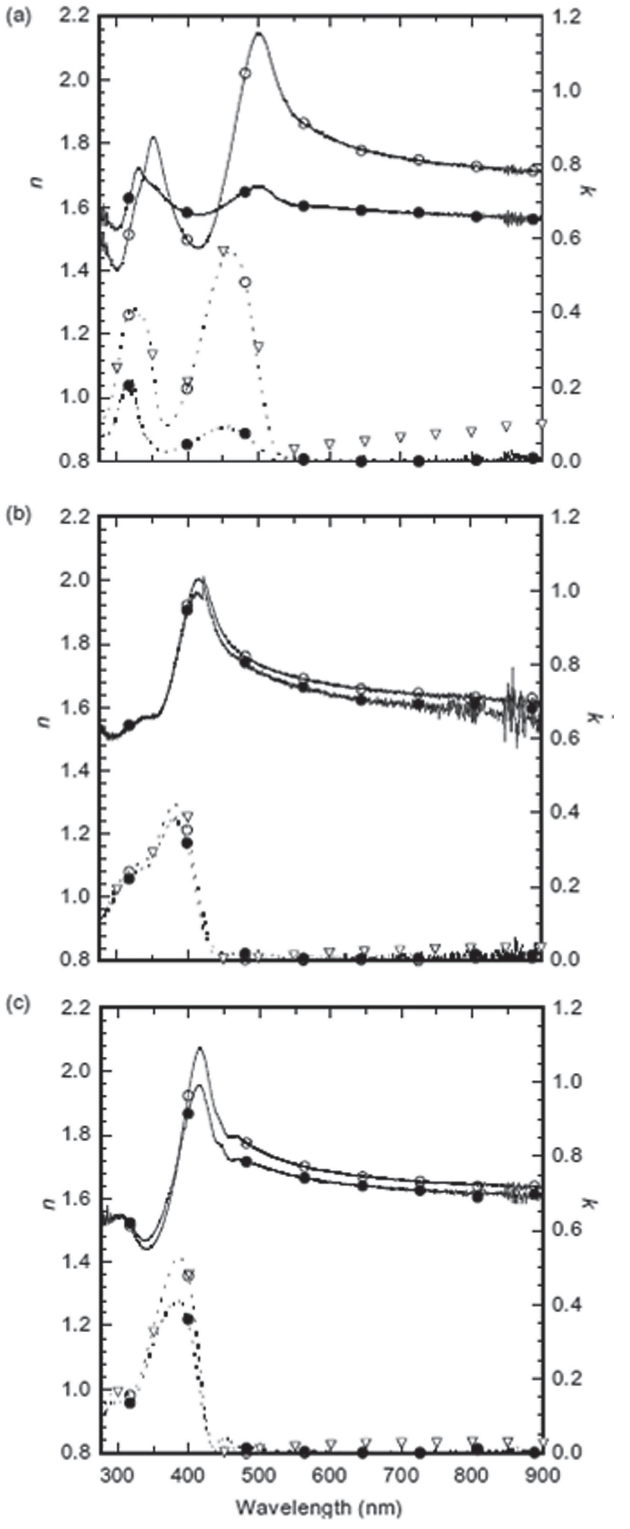

Figure 3. Anisotropic refractive index data for a) F8BT, b) TFB, and c) PFB thin film samples subjected to thermal treatment. Ordinary (in plane) indices are shown with open symbols, while extraordinary indices (out of plane) are shown with filled symbols. The anisotropy is substantially larger for F8BT than either of the arylamine copolymers. F8BT is a thermotropic liquid crystal whereas TFB and PFB are not. Reproduced with permission.[9] Copyright 2003, Institute of Physics Publishing.

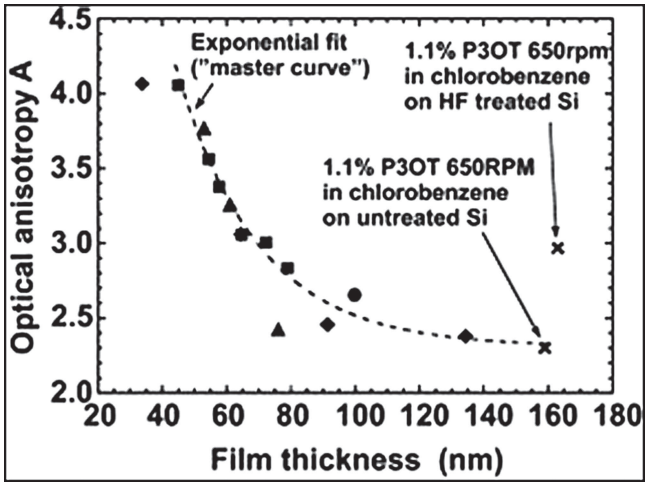

Figure 4. Optical anisotropy defined as the ratio of the imaginary parts of $\varepsilon_{||}$ and ε at their maxima as a function of film thickness for P3OT films deposited with different spin speeds on glass substrates (triangles) and on untreated silicon (squares), and also from different solution concentrations (diamonds). Reproduced with permission.[22] Copyright 2004, Elsevier B. V.

degree of anisotropy depends on the fabrication conditions.[22,25] For spin coated films, the drying rate is determined by the solvent vapor pressure and spin speed, while the total drying time is set by the solution concentration and final film thickness. For P3OT, as shown in **Figure 4**, the anisotropy appears to depend largely on final thickness but note the significant difference accorded by surface energy treatment (HF treated Si vs untreated Si). This, however, may depend on the particular material system. For instance, it has been recently reported that for MEH-PPV there is no film thickness dependence of the optical properties in the thickness range between 18 nm and 178 nm.[92] It has also been shown that long film deposition times, for example, by using drop casting (i.e., placing a drop of solution onto a substrate and waiting for it to dry) instead of spin coating as the deposition method, can result in much larger anisotropies for some materials.[22] It is often observed that the degree of anisotropy varies depending on the substrate (and any surface treatments administered thereto) upon which the film is deposited as is also seen in Figure 4. This may be due to templating arising from free energy considerations at the film/substrate interface and/or ordering due to the difference in free energy at the top film/air interface versus that at the film/substrate interface.

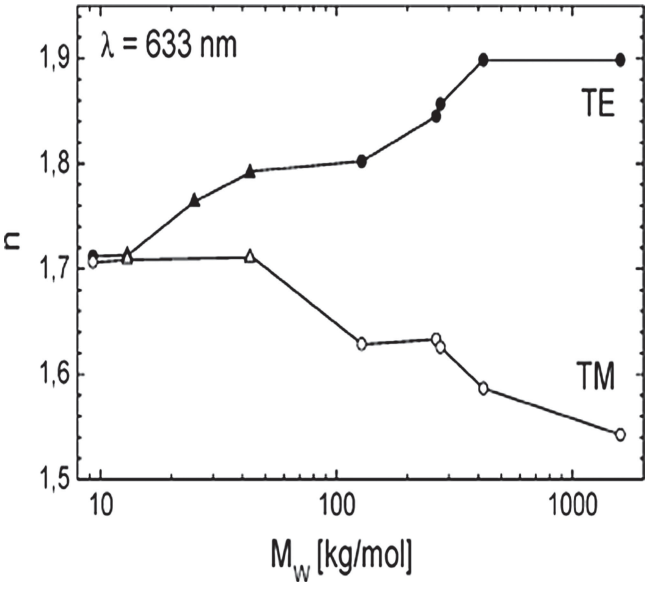

Figure 5. Optical anisotropy, *n*, plotted as a function of molecular weight for MEH-PPV films. Anisotropy values were deduced from prism coupling and reflectivity data. TE (TM) index corresponds to n_o (n_e) in this paper. Reproduced with permission.[20] Copyright 2006, American Chemical Society.

Molecular weight, M_w, also appears to have a strong effect on the resulting anisotropy.[20,21,93] For the case of MEH-PPV films, the difference $n_o - n_e$ decreases from 0.35 at $M_w = 10^6$ g mol^{-1} down to almost zero for films fabricated with $M_w = 10^4$ g mol^{-1}.[20] **Figure 5** shows this dependence. The same trend has been observed for F8BT films.[93] One difficulty here is that M_w can be a proxy for other factors such as the degree of chain entanglement, the type of chain packing, the number of defects, and so forth, and it is then necessary to unravel these contributions before one can draw any more general conclusions. The specific side chains that are attached to the conjugated backbone also affect the optical properties and anisotropy.[45,94,95] In addition, end groups will play a role.[96]

These dependences on deposition conditions and molecular weight may partially explain the large discrepancy in the values of anisotropy found in early work on the optical properties of conjugated polymer films. For instance, in the case of MEH-PPV, $n_o - n_e$ values at ≈525 nm as small as 0.008[76] and as large as 0.7[97] have been reported. It then becomes clear that, for quantitative modeling of polymer-based systems, it is necessary for each laboratory to develop reference optical functions based on their specific processing conditions.

Besides materials related issues, it has been pointed out that conventional ellipsometry alone is not sensitive enough to reliably derive the out-of-plane complex refractive index of organic semiconducting thin films.[30,78] Other slightly more sophisticated techniques have been proposed instead. These include the combination of reflection VASE and transmittance,[32,33] reflection and transmission VASE,[9,78] using multiple sample analysis[22,25,34,35,80] or interference enhancement VASE.[30,81,98] In a recent collaborative investigation, Campoy-Quiles et al. have shown that the above techniques all result in comparable optical constants and anisotropy, also in good agreement with prism coupling waveguiding techniques.[81] In this round-robin study, samples of PVK were prepared at one institution and sent to six other groups around Europe. The results of this study suggest that the large spread among the reported values of optical anisotropy in the literature may derive from lack of reproducibility of the film fabrication, in many cases due to a lack of explicit information on important issues such as polymer molecular weight or film thickness. Or, in other words, combined or more sensitive experiments do allow the anisotropy to be reliably deduced using ellipsometry. Most important then is that when quoting anisotropy values of a polymer film,

careful attention should be placed on managing and reporting the material characteristics and fabrication conditions.

Our experience suggests that multi-sample or multi-technique analysis helps to de-correlate the fitting parameters and obtain a more precise description of the complex structure of the films, possibly including substrates with a high index contrast relative to the organic films.[30] Moreover, we have found that during the fitting process for the transparency region of anisotropic films, the convergence is often more stable if a change of fitting variables is made, from n_o and n_e to an average index, <n>, and an index difference, δ:

$$< n >= \frac{n_o + n_e}{2} \tag{5}$$

and

$$\delta = \frac{n_o - n_e}{2} \tag{6}$$

A quantitative analysis of the anisotropy of the dielectric tensor can provide significant insight into film structure. A proper description of the relationship between the molecular orientation function of the transition dipoles in a film and the macroscopic dielectric tensor is complex.[99,100] However, for the range of limited variability often encountered in conjugated polymer films, a first order linear effective medium approach is typically sufficient to analyze the data. If one considers the film to be a homogeneous material, described by a local dielectric tensor $\overleftrightarrow{e}$ and an orientation distribution function $f[\Theta,\Phi,\Psi]$ (where Θ, Φ, and Ψ are the Eulerian angles depicted in **Figure 6**), then the film $\overleftrightarrow{\varepsilon}$ is given by:

$$\overleftrightarrow{\varepsilon} = \int \overleftrightarrow{U}^{-1}[\Theta, \Phi, \Psi]\, \overleftrightarrow{e}\, \overleftrightarrow{U}[\Theta, \Phi, \Psi]\, f[\Theta, \Phi, \Psi]\, \sin\Theta\, d\Theta d\Phi d\Psi \tag{7}$$

where $\overleftrightarrow{U}$ is a unitary rotation matrix. The local dielectric tensor with at least orthorhombic symmetry, if dominated by a single transition, will have the form

$$\overleftrightarrow{e} = \begin{bmatrix} e'_{ab} & 0 & 0 \\ 0 & e'_{ab} & 0 \\ 0 & 0 & e'_c + j e''_c \end{bmatrix} \tag{8}$$

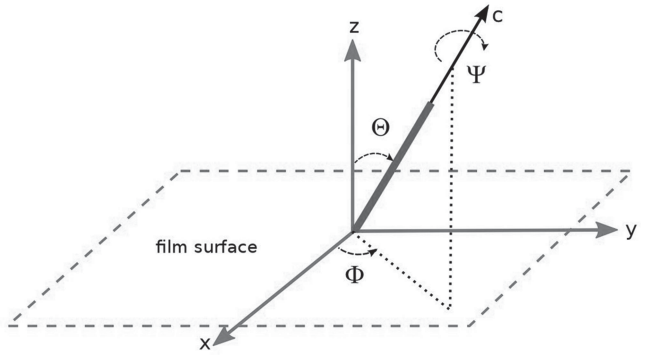

Figure 6. The orientation of the molecules in the laboratory frame (*x*,*y*,*z*) is defined by Eulerian angles Θ, Φ, Ψ, where Θ and Φ are the polar and azimuthal angles which determine the direction of the *c* axis and Ψ represents the rotation of the molecular segments about their *c* axis, which is usually chosen as the conjugated backbone.

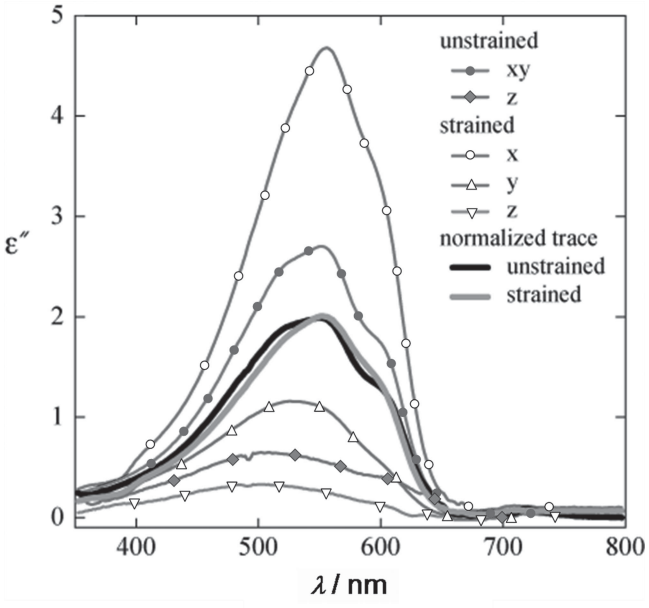

Figure 7. Imaginary part of the diagonal elements of the dielectric function, ε, for a biaxially oriented P3HT film derived from spectroscopic ellipsometry studies of 0% and 90% strained films. The used P3HT had a number average molecular mass M_n = 62kD, ($M_w = 6.2 \times 10^4$ g mol^{-1}) a regioregularity of 99%, and a polydispersion of 1.9. The films were deposited from a chloroform solution onto octyltrichlorosilane modified silicon substrate with a native oxide layer. Reprinted with permission.[111] (Supporting Information). Copyright 2011, American Chemical Society.

We note that, within the linear effective medium approach mentioned above, the trace of the dielectric tensor is conserved. For $\overleftrightarrow{e}$ of the form given by Equation 8, this implies that $\varepsilon''_x + \varepsilon''_y + \varepsilon''_z = e''_c$. Thus, ellipsometric determination of the anisotropy of $\overleftrightarrow{\varepsilon}$ is critical to any discussion of transition strengths as changes in anisotropy will affect the ubiquitous normal incidence absorption measurements. The measured normal incidence absorption coefficient can increase by a factor 1.5 from a random isotropic morphology to a uniaxial (aligned in-plane transition dipoles) morphology with no real change in intrinsic oscillator strength. Shown in **Figure 7** are the imaginary parts of the dielectric tensor of P3HT films that were biaxially oriented by a novel strain and transfer process.[101] The unstrained film shows a typical level of uniaxial order for spin coated P3HT. In the strained film, ε''_x (*x* along the strain) increases due to alignment of the long axis of the polymer whereas ε''_y decreases. Interestingly, ε''_z also decreases, implying re-orientation of out-of plane segments. Note that the traces of the tensors for the unstrained and strained films are essentially the same.

Using Equation 8 and with the further assumptions that $e'_a \approx e'_b$ and that the distribution is isotropic in Φ, measurement of the ratio $\varepsilon''_{xy}/\varepsilon''_z$ (either as integrated intensity or values taken at the maximum) can define $<\cos^2\Theta>$. For conjugated systems, one often is interested in both the chain-axis orientation $<\cos^2\Theta>$ and the π stacking orientation $<\cos^2\Psi>$. Unfortunately, for most polymer systems, the orientation of the dominant transition dipoles is along the chain axis (or equivalently, there is axial symmetry about the chain axis in most samples) and

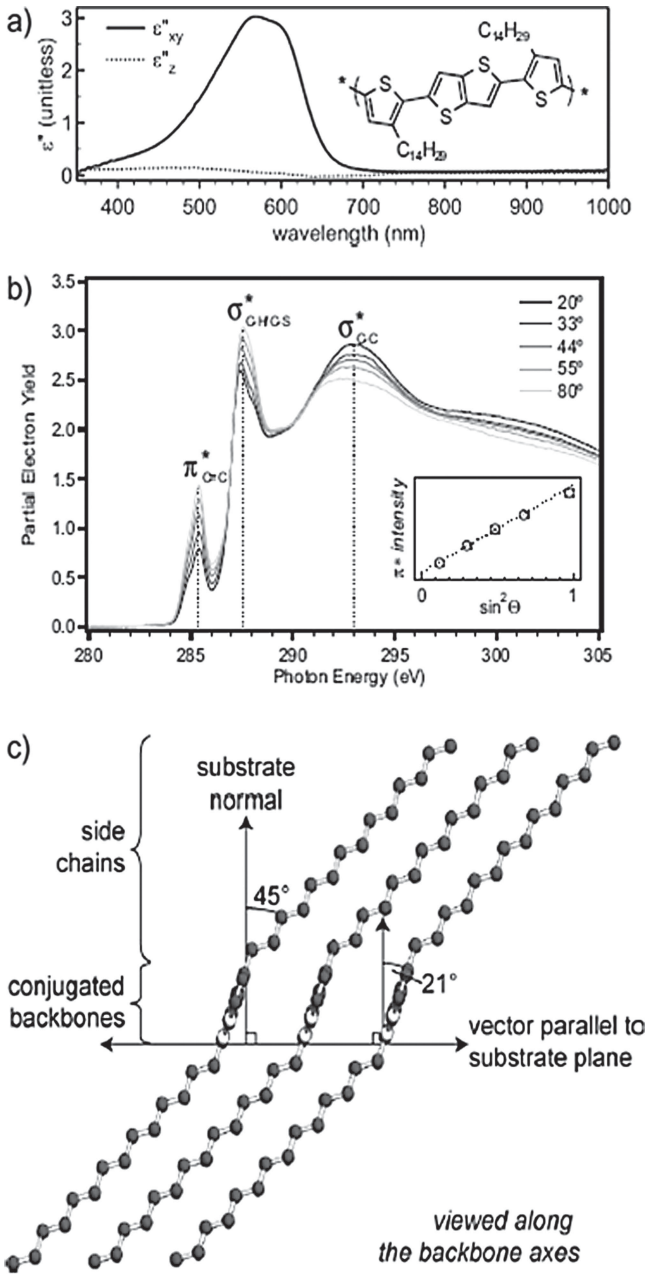

Figure 8. Determination of the packing structure of pBTT-C14 films (chemical structure in the inset to a) using two complementary measurements: a) Imaginary part of the anisotropic dielectric function. b) Carbon K-edge NEXAFS spectra at five incident angles. c) Deduced details of the packing geometry highlighting the slip stacking of the π planes. Reprinted with permission. [102] Copyright 2007, WILEY-VCH Verlag GmbH & Co. KGaA, Weinheim.

visible ellipsometry alone cannot determine both orientation functions. There is strong synergy between ellipsometry and polarized near edge X-ray absorption fine structure (NEXAFS) spectroscopy,[63,102] in that NEXAFS often has extremely good sensitivity to the orientation of the normal to the π plane. Combining the two techniques can enable a complete description of the polymer backbone orientation. Similarly, ellipsometry can be combined with structural characterization techniques such as X-ray diffraction[22,34,103] or Fourier transform infrared (FTIR)[102] and Raman[57] vibrational spectroscopies. **Figure 8** shows the results of a study of highly crystalline pBTTT films, for which excellent thin film transistor performance is achieved. Visible ellipsometry and NEXAFS were used to identify the orientation of the backbone and the slip stacking of the π–π planes. Polarized IR absorption (based on optical models informed by ellipsometry measurements) established the order and orientation of the alkyl side chains. Grazing incidence X-ray diffraction established the crystal lamella repeat distance, and combined with IR spectroscopy, the side chain interdigitation.[102] This suite of complementary measurements enabled an almost complete description of both the lattice and molecular unit cell structure.

3.3. Multi-Phase Morphology and Optical Properties

Like molecular solids, polymer systems may exhibit a diversity of solid phases: amorphous, rubbery, liquid crystalline and crystalline. Due to the constraints of chain connectivity and entanglement, a film rarely consists of a single homogenous phase at any temperature. Quite often the film will consist of ordered regions (crystallites) embedded in an amorphous (glassy) matrix.[104] Monodomain liquid crystal samples can also be prepared using rubbed polyimide alignment layers.[105,106] Furthermore, in cases where the side chains are of sufficient length, a nanophase separation can occur with the potential for the backbone and the side chains to have different levels of order, for example, glassy, liquid crystalline or semicrystalline backbones with crystalline or amorphous melt/glassy side chains.

In general, the relative amounts of each of these locally defined phases and the degree of order in the phase is a function of film processing. Rarely is the ultimate, thermodynamically stable, microstructure created in the lab. For each of the phases that exist within a film, the repeat-units may have different molecular conformations (e.g., coiled and entangled versus planar) and packing densities. As a result, the relative proportions of the different phases will determine the macroscopic optical properties of the film, both in terms of spectral content (reflecting the electronic density of states) and anisotropy (reflecting orientation).

As an example, in **Figure 9**, we show the complex refractive index for a 106 nm thick PFO film in the as-spin-coated (squares) and subsequently crystallized (circles, cooled from the melt) phases.[60] Owing to a better packing of the polymer chains in the crystalline phase, the oscillator strength is higher, evidenced here by stronger absorption and a correspondingly enhanced refractive index in the transparency region of the spectrum.

There are other examples in the literature for the optical constants of PFO processed with different thermal[107] and vapor[108] treatments, for F8BT depending on thermal history,[9] for PFO and F8BT as a function of the geometrical confinement of the substrate[26] and for polythiophenes as a function of spin coating conditions.[22,25]

Many of the changes in index of refraction can be rationalized in terms of variations in film density (ρ) and polarizability

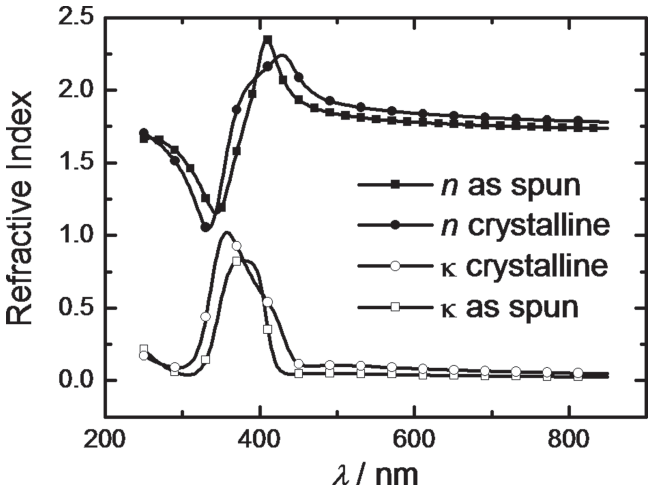

Figure 9. Refractive index, n (solid symbols), and extinction coefficient, κ (open symbols), for a PFO film as-spin-coated (squares) and after crystallization (circles), deduced using an isotropic model for the dielectric function found in the literature.[60]

(μ).[23,45,109] In the transparency region of the spectrum the variation in refractive index can be expressed as:

$$\frac{n_t^2 - 1}{n_0^2 - 1} \cong \frac{\mu_t \rho_t}{\mu_0 \rho_0} \tag{9}$$

This relationship has been used to compare density and polarizability values for samples with different side chain lengths,[45] before and after thermal annealing[57,107] and during deposition.[23]

For real time experiments during post-deposition treatment,[23,57] the film mass at two given times is conserved, and therefore the changes in density are related to film thickness changes:

$$\frac{\rho_t}{\rho_{t=0}} \cong \frac{1/d_t}{1/d_{t=0}} \tag{10}$$

Equation 9 can then be rewritten:

$$\frac{n_t^2 - 1}{n_{t=0}^2 - 1} \cdot \frac{d_t}{d_{t=0}} \cong \frac{\mu_t}{\mu_{t=0}} \tag{11}$$

Which, since the refractive index and thickness can be deduced independently during an ellipsometric experiment, allows one to estimate the changes in polarizability that occur during any treatment to optimize (or modify) the film morphology. These changes may be due, for instance, to changes in the average degree of molecular orientation during annealing.[23]

When the film is semi-crystalline, the highly ordered regions can be characterized by grazing incidence diffraction techniques. However, the evaluation of amorphous material from diffraction can be highly unreliable typically due to the large width of the amorphous halo and the difficulty to distinguish it from the background, which makes very difficult to estimate the crystalline fraction. It is frequently more reliable to resort to optical spectroscopic evaluation. In favorable cases, such as P3HT, where the crystalline phase exhibits distinct optical features, the crystalline fraction can be estimated from optical transmission and ellipsometric data.[66,110] In general, the anisotropy of the crystalline regions will be distinct from the amorphous regions. In this case, the overall anisotropy in the system can be approximately modeled as $\vec{\vec{\varepsilon}} = f_c\vec{\vec{\varepsilon}}_c + (1 - f_c)\vec{\vec{\varepsilon}}_a$, where $\vec{\vec{\varepsilon}}_c$ ($\vec{\vec{\varepsilon}}_a$) are the dielectric tensors for the crystalline (amorphous) regions and f_c the volume fraction of crystalline material. Again this linear approach can be used for the tensor components because their absolute values for the amorphous or crystalline regions will not differ much. If the individual reference tensors are available or, alternatively, diffraction or other tools can place reasonable constraints on the dichroic ratio (e.g., fraction of in-plane orientation of polymer backbones) of the individual phases, measurement of the total film anisotropy can be used to estimate the crystalline fraction of the film.[102,111]

4. Vertically Structured Films

In the previous section, we focused on thin films of a single polymer. One of the greatest strengths of ellipsometry is the ability to nondestructively depth profile vertically structured films. Thus ellipsometry is a powerful complement to higher precision techniques such as x-ray and neutron reflectivity, which are non-destructive but have limited chemical contrast (the scattering length density cannot be uniquely attributed to composition if more than two components are present) and require large samples due to the use of grazing incidence. Additionally ellipsometry complements destructive, sputter-depth-profiling techniques such as secondary ion mass spectrometry (SIMS) and X-ray photoelectron spectroscopy (XPS) that are susceptible to artefacts from selective sputtering. For successful depth profiles, ellipsometry requires optical contrast. For conjugated polymers, the transparent region of the spectrum often does not have adequate contrast, thus the technique is best suited to structures that are of the order of the absorption depth where absorption contrast can be leveraged. Precision restricts the resolution to layers typically 0.1 to 0.01 times the incident wavelength (hence the success of X-ray and neutron reflectometry). The interpretation of the data is most straightforward when accurate reference dielectric functions are available.

Vertical structure arises in conjugated polymer systems both deliberately, as in the sophisticated multilayer stacks engineered for advanced optoelectronic devices such as white OLEDs,[112] photodiodes[113] and tandem organic photovoltaic cells,[114] and adventitiously, as in surface roughness, interphases and film boundaries, and interface segregation (in multicomponent films). For optoelectronic and photovoltaic applications, accurate characterization of both the dielectric function and vertical structure are essential for the design of optimal devices, since cavity effects and anisotropy can dominate both outcoupling (spectral content and amplitude) in OLEDs and photon harvesting in solar cells.[32,115–117] Accurate modeling is critical to an understanding of the internal photon conversion efficiency[118] and can lead to novel insights.[119] Adventitious structural features (segregation layers and interphases) may be too thin to significantly impact photonic behavior, but can

dominate electrical performance as they define injection and recombination characteristics.[120]

Despite the fact that spin-coated polymers are often quite smooth, films that are crystallized by thermal annealing after deposition typically show prominent surface roughness.[57,121] The inhomogeneous surface needs to be taken into account when characterizing the optical constants of such films, as well as when attempting to understand other related properties such as photoluminescence intensity, waveguiding properties,[87,121] or even internal quantum efficiency in solar cells.

Optically, mesoscale (of the order of wavelength) surface roughness scatters incident light into different directions and can depolarize it. The greater the roughness, the more pronounced these effects are. As most ellipsometers have a long optical path, the contribution of scattered light to the detected polarization change is often negligible compared to that of the specular beam. However, scattered light can still influence results if the roughness is large. It has been noted that for polymer thin films with a roughness smaller than 10% of the total thickness, conventional ellipsometric measurements are reliable.[78] Alternatively, a full Mueller matrix ellipsometric measurement[5,6] is recommended for very depolarizing samples, with either large surface roughness or inhomogeneities within the film.

When surface roughness arises from significantly sub-wavelength features, it is often modelled as a mixed layer of the underlying material and air (see **Figure 10**, top). This layer is characterized by planar interfaces and a given volume fraction of the material with respect to air.[5] Typically, an effective medium approximation, EMA, such as that proposed by Bruggeman,[5,6,122] is used to characterize the dielectric function of this mixed layer. Some limitations of the Bruggeman theory will be discussed below but it is worth noting that, in a number of cases, detailed studies of inorganic systems do indicate good correlation between values derived from ellipsometric roughness models and AFM.[123,124]

Another important variety of diffuse interface is that which arises from mixing at the boundary between sequentially deposited polymer layers (Figure 10, middle). Such mixing is common since it is difficult to find orthogonal (incompatible) solvents for sequentially deposited layers. During the deposition of a second layer, the first one may partially (or totally) dissolve such that a mixed interfacial layer is formed. A degree of interfacial mixing can also happen for bilayers formed by thermally evaporating the top layer.[125] Provided that the dielectric functions for each of the pure materials is already known, ellipsometry can be used to characterize the interfacial layer. One such example is shown in **Figure 11**, where a bilayer structure was formed by spin coating a 300 nm thick F8DP film onto a silicon wafer and then spin coating a 200 nm thick PDMS layer on top. Analysis of the ellipsometric data for this sample confirms the presence of a PDMS-rich interlayer between the two single material layers.

Bilayer films provide important model interfaces for the study of photovoltaic devices. The appearance of interlayers is expected to be a general feature of organic bilayers, where partial miscibility between materials is often found. Ellipsometry can provide critical validation of film structure in experiments that require a sharp interface, such as the determination of the exciton diffusion length.[125] In unpublished studies undertaken

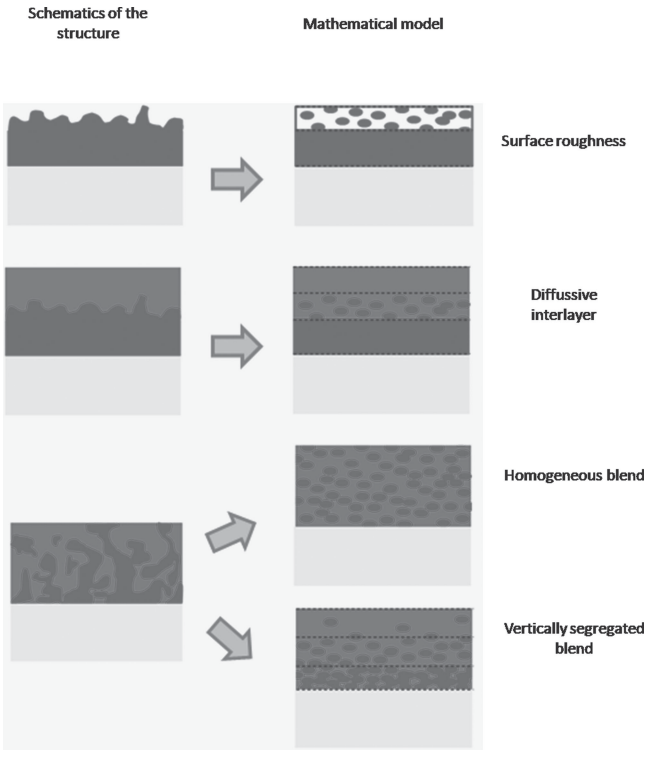

Figure 10. Schematic cross-sections (left) and idealized mathematical model cross-sections (right) for structures with surface roughness (top), a diffusive interlayer (middle), and a bulk heterojunction (bottom). For the latter, two mathematical models are shown, a homogeneous blend and a vertically segregated blend.

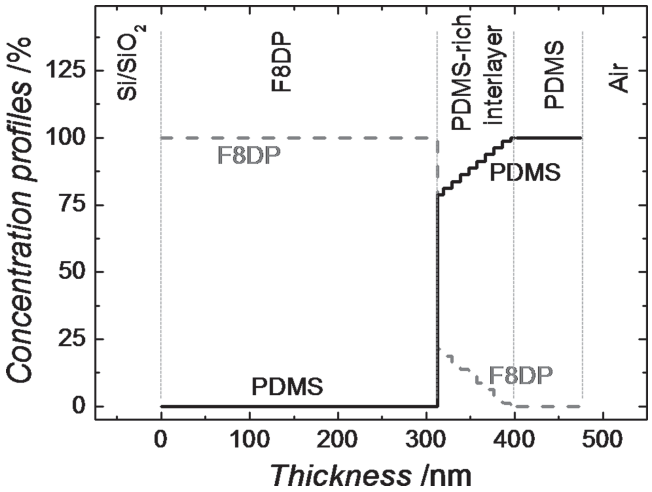

Figure 11. The concentration depth profiles for F8DP (dashed line) and PDMS (solid line) deduced using VASE for a Si/SiO_2/F8DP (300 nm)/PDMS (200 nm) sample. The SiO_2/F8DP interface is arbitrarily located at a thickness value of 0 nm and the ellipsometry data reveals the presence of a mixed (predominantly PDMS) layer of ≈100 nm thickness on top of the F8DP layer. Dotted lines are guides to the eye representing the boundary of the different layers.

in one of the current author's laboratories it has been found that solvent casting the soluble fullerene PCBM from a nominally orthogonal solvent (dichloromethane) on top of P3HT leads to a significant (≈15%), uniform penetration into the underlying polymer. This SE study is supported by a recent neutron reflectivity report.[126] Ferenczi et al. previously used VASE to explore interdiffusion for a P3HT/PCBM bilayer system.[127] The distinguishing feature of this work was that the top layer was deposited using a solvent free stamp transfer process. Interestingly, the authors found that there was little mixing for the as-prepared bilayers, but thermal annealing caused the fullerene molecules to diffuse into the P3HT film and form a broad mixed layer separating the two, single component, capping layers. This triple stack was found to perform as a photodiode much better than the as-prepared bilayers, and the spectral response of the photodiode was successfully modelled using vertical profiles deduced from a Bruggeman analysis of the ellipsometric data.[127]

Next, we discuss the case where a mixed layer is formed by spin coating a solution already containing two materials, as this is the protocol normally employed to form the technologically relevant bulk heterojunction structure (Figure 10, bottom). In principle, the optical properties of such a blend film can be modelled using an EMA (often the Bruggeman model). Our own experience,[128] as well as other reports in the literature,[129] suggests that extreme care must be exercised when using EMA models for these systems because some of the assumptions made may not be valid. In most cases, the primary assumptions of an EMA model are robust. These include the fact that the components are mixed on a fine (<0.1 wavelength) scale and that new (interface charge transfer) optical excitations are negligible.[130] However, the process of mixing leads to microstructures for the domains of the pristine materials that are not necessarily equivalent to those of the single material films from which reference dielectric functions are obtained. For instance, the degree of anisotropy or the amount of crystallinity may change. Moreover, as most organic materials are partially miscible,[131] in reality a ternary system is formed, consisting of approximately pure domains of both materials plus a fine blend of the two. More advanced models including anisotropic inclusions,[132] effective ternary mixing,[110,128,133] and so forth, will need to be employed or further developed in order to deduce the dielectric function of the blends based on those of the pure materials. Currently, the most accurate option is, probably, to treat the blend film as if it were a completely new material system (similar to an alloy) and deduce its particular dielectric function like any other material.[32,134] That having been said, the dielectric function is also likely to be spatially varying due to the heterogeneity present within the film, with the degree of spatial averaging dependent on the measurement spot size.

Despite not being always the most accurate description, use of the dielectric function of the pristine materials in the modelling of blends opens up the possibility to investigate variations across the film thickness. For instance, VASE has been employed to explore vertical segregation in blends of P3HT and PCBM[57,110,135] and other photovoltaic blends such as APFO3:PCBM[128] and PCPDTBT:PC70BM.[136] In order to perform this analysis, the blend film was modelled as a number of sublayers, each with a different composition of the two materials and the corresponding dielectric function of each sublayer deduced using an EMA model. Interestingly, it was found that as-spin-coated films already exhibited a degree of phase separation in the vertical direction, and that this segregation increased with thermal and vapor annealing.[57] Moreover, it was shown using ellipsometry that the specific depth profile depended on a variety of factors, including the hydrophilicity of the substrate,[57,134] the processing history,[57] the polymer crystallinity,[137] and the blend composition ratio.[128,135] The vertical segregation has now been confirmed by multiple techniques.[120,136–139]

In general the influence of thin (≈10 nm) interface layers on ellipsometry is subtle. Thus it is best practice to construct flexible material functions, as are often used in the treatment of alloys,[128] based on libraries of reference films processed in diverse ways. This should allow sufficiently accurate modelling of both the anisotropy and the morphology to extract detailed profiles.[134] Very recently, the vertical concentration profiles of conducting PEDOT:PSS layers (in which there is a component of un-complexed PSS) have also been investigated using ellipsometry.[140]

5. In-Situ Ellipsometry for Monitoring Film Deposition and Structural Changes

As a nondestructive and relatively fast (measurement time ≤1 s) technique, ellipsometry can be adapted for in-situ measurements of changes in film properties and this modality has been utilized mainly to study film deposition processes, changes induced by post-deposition treatments and phase transition temperatures in thin films. In this section, we describe results for each of these topics.

As the amount of experimental data quickly increases for real time experiments, the analysis required can be challenging. For this reason, we start the discussion by briefly discussing information that can be drawn directly from the raw ellipsometric angles.

An important observation is that for relatively small changes in morphology and thickness, such as those normally caused by thermal annealing, the ellipsometric parameters typically vary approximately linearly with film thickness. The relative sensitivity of Ψ and Δ to thickness and the sign of the relationship depend on the specifics (thickness, dielectric constant, substrate, angle of incidence). This is illustrated in **Figure 12** for three different materials, APFO3,[128,131] PFO,[26,121] and P3HT.[57] In these cases, the films were thermally annealed while recording ellipsometry data. The raw data were fitted and the thicknesses deduced, allowing plots of thickness *vs* Ψ to be constructed. Note the change in sign of the slope between the Si and fused silica substrates.

This observation opens the possibility of extracting insight directly from the raw ellipsometry data. As an example, we show in **Figure 13** the evolution of $\tan\Psi$ at 550 nm for a ≈102 nm thick PFO film on quartz during several temperature cycles (heating/cooling at a rate of 0.7 °C min^{-1}). Figure 13a focuses on the lower temperature region, where a kink in $\tan\Psi$ is observed around the glass transition temperature (T_g) on heating. T_g can

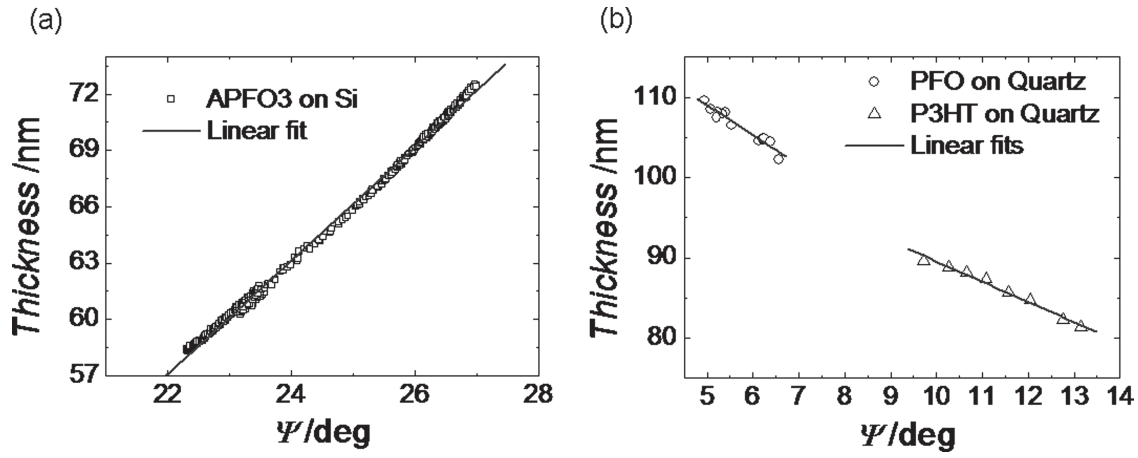

Figure 12. Correlation between the ellipsometric angle $\Psi \approx \tan\Psi$ (measured at a wavelength in the transparency region) and the film thickness for a) the low band gap polymer APFO3 deposited on silicon;[131] and b) PFO[55] and P3HT[57] on quartz. Straight lines correspond to linear fits. Data were collected in each case during the thermal annealing of spin-coated films.

be determined by obtaining the intersection of two straight-line fits to the data below and above the kink. In this case T_g = 54 °C is in good agreement with differential scanning calorimetry (DSC) measurements. [55,121,141] For a given material, the clarity of the kink for a particular sample will depend on a number of factors such as film thickness, supporting substrate material and heating rate. Interestingly, the realization that $\Psi \propto d$, helps to interpret this kink as a change in the thermal expansion coefficient of the film before and after the glass transition.[142]

Other authors[131,143–145] have used the raw ellipsometry data (Ψ and Δ) to directly extract T_g for polymeric films. For instance, the T_g values obtained for polystyrene films using directly Ψ and Δ or the deduced film thickness and refractive index after data analysis have been found to agree to within one degree Celsius.[146]

By increasing the temperature further, a rubbery film may undergo crystallization. In the raw ellipsometric data, the crystallization of PFO (when supported on quartz) is manifested as an abrupt rise in $\tan\Psi$ (see Figure 13b), which is equivalent to saying that the film thickness (density) rapidly decreases (increases) upon crystallization (c.f. Figure 12b). Quartz supported F8BT films show similar behavior,[26] namely a kink in $\tan\Psi$ around T_g, followed by a sudden increase in $\tan\Psi$ at the crystallization temperature (T_c), or more correctly, the temperature of maximum crystallization rate.

The nominal value for T_c can be obtained at the inflection point of $\tan\Psi$ versus T in analogy with the maximum of the exothermic peak in a DSC experiment. The width of the transition (analogous to the width of the DSC peak) can be defined by the onset and offset of the step (T_{c1} and T_{c2} in Figure 13b). For this 102 nm thick PFO film, the crystallization temperature is found to be T_c = 84 °C, with a crystallization width $\Delta T_c = T_{c2} - T_{c1} = 4$ °C.

The in-situ capabilities of ellipsometry can be used to fully characterize phase behavior in quasi-isothermal experiments. Shown in **Figure 14** are results from a temperature dependent study of pBTTT.[147] As discussed earlier, pBTTT is a highly crystalline polymer. It also exhibits a broad liquid-crystal (LC) phase transition near 150 °C. Transistor performance is greatly improved by annealing films in the LC phase. Shown in Figure 14a is the thickness of a nominally 25 nm film as a function of temperature. As in the preceding PFO studies, the phase transition can be identified by the inflection point, centered near 140 °C. Annealing in the liquid crystal phase allows removal of defects in the initial, as-spin-coated, evident in the increase in film density (lower thickness) upon cooling from the LC phase. Shown in Figure 14b is the film anisotropy (from an in-situ multi-sample experiment) characterized by the ratio between the out-of-plane integrated ε''_z to the in-plane ε''_{xy} . The degree of anisotropy increases with temperature and is improved by the annealing cycle. Figure 14c shows the peak

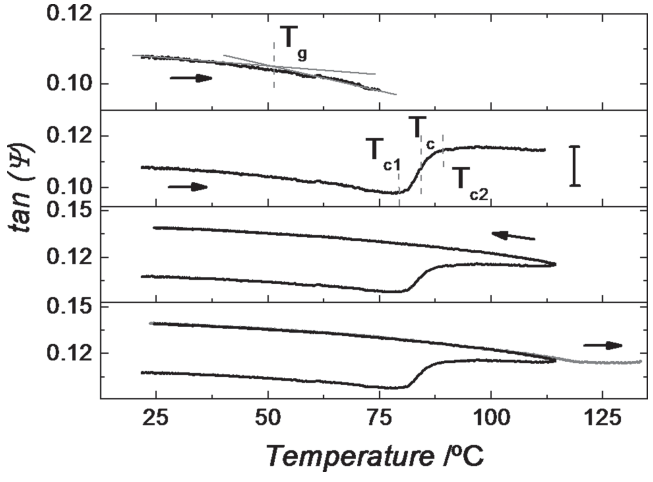

Figure 13. Raw ellipsometry data at 550 nm as a function of temperature for a 102 nm thickness PFO film on a quartz substrate. Top: The low temperature range on heating; the observed kink corresponds to T_g. Second from top: $\tan\Psi$ shows a step change (ΔT_c) on crystallization during heating. Second from bottom: The value of $\tan\Psi$ does not revert on cooling. Bottom: A memory effect is evident on re-heating.

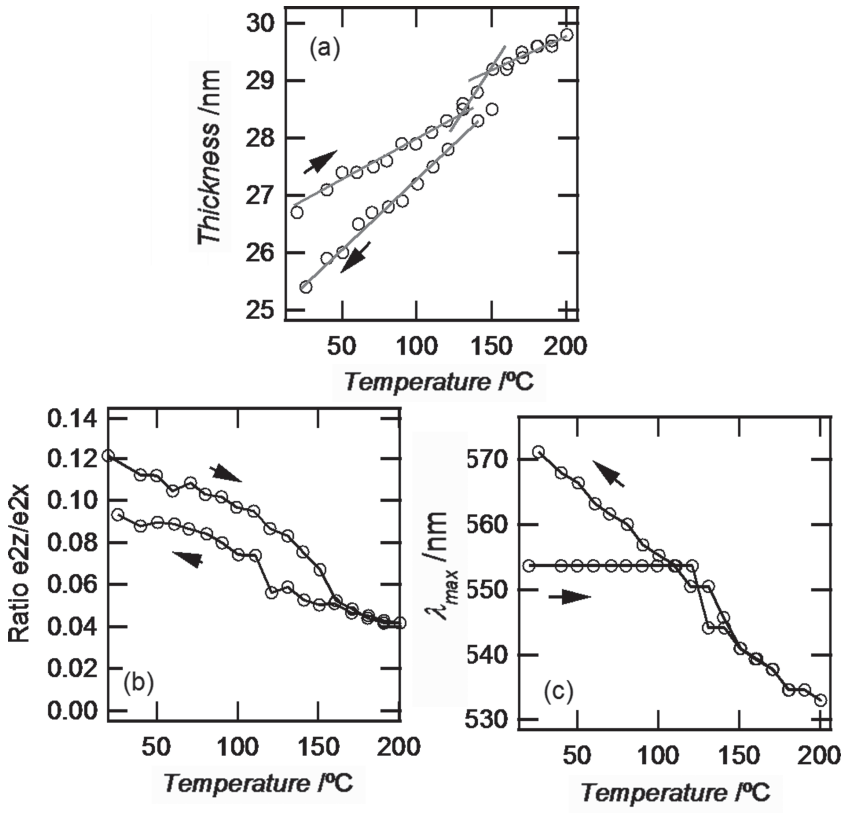

Figure 14. Results from an in-situ ellipsometry study of the annealing of pBTTT thin films. a) Film thickness variation indicating the liquid crystal phase transition near 140 °C. b) Anisotropy in the imaginary part of the dielectric function. c) Peak absorbance wavelength. Reproduced (adapted) with permission. [147] Copyright 2008, American Chemical Society.

wavelength for the in-plane absorption spectrum. The spectrum is initially nominally independent of temperature, attributed to torsional disorder that arises during spin coating. Upon entry into the LC phase, monotonic thermochromism is observed, and maintained during the entire cooling cycle. The improved order after annealing is also manifest in the large red shift on cooling.

The heating and cooling cycles shown in Figures 13, 14 exhibit typical thermal behavior of polymers as often revealed by DSC. There is irreversibility between heating and cooling since the film has a memory of the previous path; it thermally stabilizes to the maximum temperature to which it was last taken.[57,60] Only when taken to a higher temperature in a subsequent cycle will the temperature dependence be possibly changed. The main advantage of using ellipsometry with respect to DSC is that one can monitor the phase behavior directly in technologically relevant geometries such as thin films (c.f. bulk sample requirements for conventional DSC), which is important as the phase transitions may depend on the geometrical confinement imposed by the thin film structure.[26] Interestingly, it has been found that the glass and crystalline phase transition temperatures of PFO and F8BT thin films strongly depend on the film thickness.[26] This finding suggests that in conjugated polymer films there exists a profile of phase transition temperatures through the thickness of the film, similar to what has been observed in other, non-conjugated polymer films.[148,149] Comparison between thermal transition temperatures deduced at the surface (using temperature dependent AFM) and in the bulk (via Raman) have confirmed higher temperature values at the surface.[150] Very recently, we have developed a method to analyse temperature dependent spectroscopic ellipsometric data to deduce full phase transition depth profiles and demonstrate its use for thin films of PFO, APFO3, APFO9, and P3HT.[151] Interestingly, all of these systems exhibit higher transition temperatures at the free surface, contrary to what typically occurs for silica supported films of non-conjugated polymers.[148,149]

Recently, the phase diagram for bulk heterojunction films of the low band gap polymer APFO3 and fullerene (PCBM), of interest for solar cells, has been deduced using ellipsometry.[131] For this, the evolution of the ellipsometric angles as a function of temperature was measured for different polymer: fullerene compositions. The phase diagram observed in this system is similar to that found for polythiophene:PCBM blends using DSC.[152]

In-situ ellipsometry during thermal and other treatments can offer new insights into morphology evolution. We have recently shown, for instance, that when a P3HT:PCBM bulk heterojunction is exposed to a saturated atmosphere of solvent vapor, the polymer chains start to crystallize.[57] This was deduced from changes in oscillator strength (and density) that are evident in the ellipsometry data. Lateral and vertical diffusion of fullerene molecules then follows[57,109,135] and yields a blend structure that offers superior solar cell performance.

Very recently, Wang et al. have made an exhaustive ellipsometric investigation of the thermal annealing of P3HT:PCBM blends, and were able to identify three distinct regimes, namely, the evaporation of the solvent trapped within the film, the crystallization of the polymer and the phase separation of the two components.[153]

The time scale of the microstructural changes during thermal or vapor annealing is typically relatively long; changes occur over several minutes. More challenging is the characterization of thin film changes during fast deposition processes. Recently, several groups have been able to investigate deposition methods such as dip-[23] and knife-coating[24,154] and even spin-coating of non-conjugated polymer blends has been monitored using high speed photometry.[155] The layer-by-layer growth of small molecule films has also been recently monitored using polarized photometry.[156]

In a combined in-situ ellipsometry and X-ray investigation, the different steps of the drying kinetics of a P3HT:PCBM film deposited by knife-coating have been identified.[24] This encouraging report shows that once the concentration of polymer in

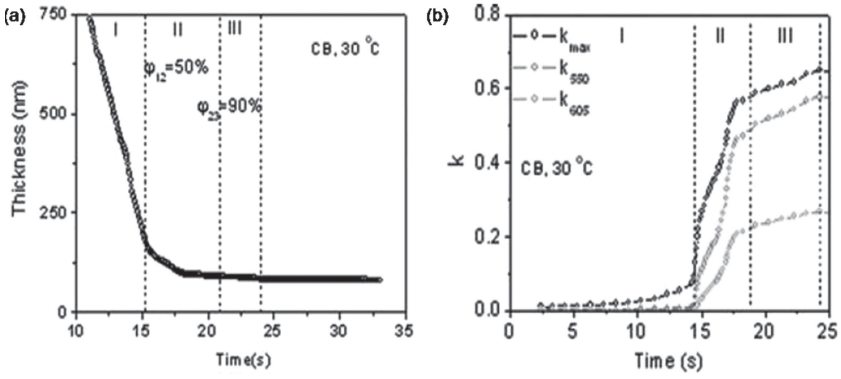

Figure 15. Ellipsometrically deduced a) film thickness and b) extinction coefficient, κ, at the peak wavelength (k_{max}) and at 550 (k_{550}) and 605 nm (k_{605}) for a P3HT:PCBM blend film during deposition by knife-coating from chlorobenzene at 30 °C. The three different regimes, I, II, and III are delineated with vertical dashed lines. Reproduced with permission.[24] Copyright 2010. Royal Society of Chemistry.

the wet film increases above 50%, the polymer chains start to crystallize via heterogeneous nucleation. A self-annealing step occurs due to the remaining solvent within the film. This is illustrated in **Figure 15**, by changes in film thickness and extinction coefficient, κ, as deduced using VASE.[24]

Clearly, the use of in-situ ellipsometry for the characterization of conjugated polymer films upon annealing or during deposition is still at an early stage of development, but very promising results have already been reported, encouraging further investigations. In particular, it could represent a very powerful technique to understand the molecular kinetics during film formation and post-deposition treatments, as well as for the in-situ characterization of layers and stacks during roll-to-roll processing.[7,8]

6. Conclusion

An accurate knowledge of the dielectric functions of semiconducting polymer films, such as obtained using ellipsometry, is fundamental to our ability to model and understand the optoelectronic properties of devices based on this family of materials. Moreover, advanced ellipsometry can be used to obtain valuable information about the structure of the thin films, as well as the quality of interfaces, phase separation of components and molecular kinetics. Here, we have reviewed a selection of the most relevant results concerning the use of spectroscopic ellipsometry for the characterization of semiconducting polymer films. First, we have shown that asymmetric lineshapes of the dielectric function, such as excitons, provide the best fits to ellipsometry data and that one should employ multi-sample analysis (using different substrates) to achieve an accurate determination of film anisotropy. We have further described the use of ellipsometry for the characterization of vertically structured films, both multi-layers and single layer blends. Finally, recent advances in the use of real time in situ ellipsometry to monitor film deposition processes and post-deposition treatments have been reviewed.

Acknowledgements

The authors thank Bernhard Dörling (ICMAB), Dr. Miquel Garriga (ICMAB), Prof. Alejandro R. Goñi (ICMAB), Prof. Pablo Etchegoin (Victoria University, NZ), C. Müller (Chalmers University of Technology, Sweden), Paul Stavrinou (Imperial College London), and Prof. Jenny Nelson (Imperial College London) for very useful discussions and comments. The authors also thank Dr. Colin Belton (Imperial College) for fabricating the F8DP/PDMS bilayer structures (Figure 11). M.C.-Q. thanks the Spanish Ministerio de Economía y Competitividad for funding through projects MAT2009–10642, CSD2010–00044 (Consolider NANOTHERM) and MAT2012–37776. D.D.C.B. is the Lee-Lucas Professor of Experimental Physics and acknowledges financial support from the EPSRC via the Active Plasmonics (EPSRC EP/H000917/1) and Hypix (EPSRC EP/F061609/1) grants.

APPENDIX

APFO3	poly[(9,9-dioctylfluorenyl-2,7-diyl)-*co*-5,5-(4′,7′-di-2-thienyl-2′,1′,3′-benzothiadiazole]
APFO9	poly[2,7-(9,9-dioctylfluorene)-*alt*-5,5-(5,10-di-2-thienyl-2,3,7,8-tetraphenyl-pyrazino[2,3-g]quinoxaline)]
PET	poly(ethylene terephthalate)
PEN	poly(ethylene napthalate)
PEDOT:PSS	poly(3,4-ethylenedioxythiophene):poly(styrenesulfonate)
PFO	poly(9,9-dioctylfluorene)
PFB	poly(9,9-dioctylfluorene-co-bis(*N*,*N*′-(4,butylphenyl)) bis(*N*,*N*′-phenyl-1,4-phenylene)diamine)
TFB	poly(9,9-dioctyl-fluorene-co-*N*-(4-butylphenyl)-diphenylamine)
F8BT	poly(9,9-dioctylfluorene-co-benzothiadiazole)
F8DP	poly(9,9-dioctylfluorene-co-9,9-di(4-methoxy)phenylfluorene)
P3HT	poly(3-hexylthiophene)
P3OT	poly(3-octylthiophene)
pBTTT	poly(2,5-bis(3-alkylthiophen-2-yl)thieno[3,2-b]thiophene)
PVK	poly(vinylcarbazole)

Received: September 2, 2013
Revised: October 19, 2013
Published online: December 5, 2013

[1] A. A. Virkar, S. Mannsfeld, Z. Bao, N. Stingelin, *Adv. Mater.* **2010**, *22*, 3857–3875.
[2] a) J. H. Burroughes, D. D. C. Bradley, A. R. Brown, R. N. Marks, K. D. Mackay, R. H. Friend, P. L. Burn, A. B. Holmes, *Nature* **1990**, *347*, 539–541; b) R. H. Friend, R.W. Gymer, A. B. Holmes, J. H. Burroughes, R. N. Marks, C. Taliani, D. D. C. Bradley, D. Dos Santos, J.-L. Brédas, M. Lögdlund, W. R. Salaneck, *Nature* **1999**, *397*, 121–128.
[3] C. J. Brabec, J. R. Durrant, *MRS Bull.* **2008**, *33*, 670–675.
[4] R. Azzam, N. Bashara, *Ellipsometry and Polarized Light*, Elsevier, North Holland **1977**.
[5] H. G. Tompkins, E. A. Irene, *Handbook of Ellipsometry*, William Andrew Publishing, Springer, Heidelberg **2005**.
[6] H. Fujiwara, *Spectroscopic Ellipsometry Principles and Applications*, Wiley, Chichester **2007**.
[7] M. V. Madsen, K. O. Sylvester-Hvid, B. Dastmalchi, K. Hingerl, K. Norrman, T. Tromholt, M. Manceau, D. Angmo, F. C. Krebs, *J. Phys. Chem. C* **2011**, *115*, 10817–10822.

[8] S. Logothetidis, D. Georgious, A. Laskarakis, C. Koidis, N. Kalfagiannis, *Sol. Energy Mater. Sol. Cells* **2013**, *112*, 144–156.
[9] C. M. Ramsdale, N. C. Greenham, *J. Phys. D: Appl. Phys.* **2003**, *36*, L29–L34.
[10] R. A. Synowicki, *Thin Solid Films* **1998**, *313–314*, 394–397.
[11] H. Hoppe, N. S. Sariciftci, D. Meissner, *Mol. Cryst. Liq. Cryst.* **2002**, *385*, 113–119.
[12] S. Logothetidis, *Rev. Adv. Mater. Sci.* **2005**, *10*, 387–397.
[13] A. Hinderhofer, U. Heinemeyer, A. Gerlach, S. Kowarik, R. M. J. Jacobs, Y. Sakamoto, T. Suzuki, F. Schreiber, *J. Chem. Phys.* **2007**, *127*, 194705.
[14] S. Tavazzi, M. Campione, *Appl. Phys. Lett.* **2006**, *88*, 071918.
[15] M. I. Alonso, M. Garriga, N. Karl, J. O. Ossó, F. Schreiber, *Org. Electron.* **2002**, *3*, 23–31.
[16] U. Heinemeyer, A. Hinderhofer, M. I. Alonso, J. O. Ossó, M. Garriga, M. Kytka, A. Gerlach, F. Schreiber, *Phys. Status Solidi A* **2008**, *205*, 927–930.
[17] A. B. Djuriši , C. Y. Kwong, T. W. Lau, E. H. Li, Z. T. Liu, H. S. Kwok, L. S. M. Lam, W. K. Chan, *Appl. Phys. A* **2003**, *76*, 219–223.
[18] W. Xie, Y. Zhao, J. Hou, S. Liu, *Jpn. J. Appl. Phys.* **2003**, *42*,1466–1469.
[19] M. I. Alonso, M. Garriga, J. O. Ossó, F. Schreiber, E. Barrena, H. Dosch, *J. Chem. Phys.* **2003**, *119*, 6335–6340.
[20] K. Koynov, A. Bahtiar, T. Ahn, R. M. Cordeiro, H. H Hörhold, C. Bubeck, *Macromolecules* **2006**, *39*, 8692–8698.
[21] K. Koynov, A. Bahtiar, T. Ahn, C. Bubeck, H. H. Hörhold, *Appl. Phys. Lett.* **2004**, *84*, 3792–3794.
[22] U. Zhokhavets, G. Gobsch, H. Hoppe, N. S. Sariciftci, *Thin Solid Films* **2004**, *451 –452*, 69–73.
[23] M. Campoy-Quiles, M. Schmidt, D. Nassyrov, O. Peña-Rodríguez, A. R. Goñi, M. I. Alonso, M. Garriga, *Thin Solid Films* **2011**, *519*, 2678–2681.
[24] T. Wang, A. D. F. Dunbar, P. A. Staniec, A. J. Pearson, P. E. Hopkinson, J. E. MacDonald, S. Lilliu, C. Pizzey, N. J. Terrill, A. M. Donald, A. J. Ryan, R. A. L. Jones, D. G. Lidzey, *Soft Matter* **2010**, *6*, 4128–4134.
[25] D. M. DeLongchamp, B. M. Vogel, Y. Jung, M. C. Gurau, C. A. Richter, O. A. Kirillov, J. Obrzut, D. J. Fischer, S. Sambasivan, L. J. Richter, E. K. Lin, *Chem. Mater.* **2005**, *17*, 5610–5612.
[26] M. Campoy-Quiles, M. Sims, P. G. Etchegoin, D. D. C Bradley, *Macromolecules* **2006**, *39*, 7673–7680.
[27] U. Rauscher, H. Bässler, D.D.C. Bradley, M. Hennecke, *Phys. Rev. B* **1990**, *42*, 9830–9836.
[28] K. Pichler, D. A. Halliday, D. D. C. Bradley, P.L. Burn, R. H. Friend, A. B. Holmes, *J. Phys.: Condens. Matter* **1993**, *5*, 7155–7172.
[29] J. Cornil, D. Beljonne, Z. Shuai, T. Hagler, D. D. C. Bradley, I. Campbell, J.-L. Brédas, C. W. Spangler, K. Müllen, *Chem. Phys. Lett.* **1995**, *247*, 425–432.
[30] M. Campoy-Quiles, P. G. Etchegoin, D. D. C. Bradley, *Phys. Rev. B* **2005**, *72*, 045209.
[31] B. Johs, C. M. Herzinger, *Thin Solid Films* **2004**, *455*, 66–71.
[32] N. K. Persson, H. Arwin, O. Inganäs, *J. Appl. Phys.* **2005**, *97*, 034503.
[33] A. Ng, C. H. Li, M. K. Fung, A. B. Djuriši , J. A. Zapien, W. K. Chan, K. Y. Cheung, W. Y. Wong, *J. Phys. Chem. C* **2010**, *114*, 15094–15101.
[34] T. Erb, S. Raleva, U. Zhokhavets, G. Gobsch, B. Stühn, M. Spode, O. Ambacher, *Thin Solid Films* **2004**, *450*, 97–100.
[35] M. Tammer, A. P. Monkman, *Adv. Mater.* **2002**, *14*, 210–212.
[36] D. E. Aspnes, *J. Opt. Soc. Am.* **1980**, *70*, 1275–1277.
[37] R. Rosa, *Inverse Problems* **1988**, *4*, 887–900.
[38] M. I. Alonso, M. Garriga, *Thin Solid Films* **2004**, *455–456*, 124–131.
[39] P. Drude, *Ann. Phys. Chem. N. F.* **1889**, *36*, 865–897.
[40] J. W. Weber, T. A. R. Hansen, M. C. M. van der Sanden, R. Engeln, *J. Appl. Phys.* **2009**, *106*, 123503.
[41] P. Lautenschlager, M. Garriga, L. Vina, M. Cardona, *Phys. Rev. B* **1987**, *36*, 4821.
[42] S. Adachi, *Phys. Rev. B* **1987**, *35*, 7454.
[43] M. Schubert, C. Bundesmann, G. Jakopic, H. Maresch, H. Arwin, N. C. Persson, F. Zhang, O. Inganäs, *Thin Solid Films* **2004**, *455–456*, 295–300.
[44] E. Nolot, A. Andre, *Thin Solid Films* **2011**, *519*, 2782–2786.
[45] M. Campoy-Quiles, G. Heliotis, R. Xia, M. Ariu, M. Pintani, P. G. Etchegoin, D. D. C. Bradley, *Adv. Funct. Mater.* **2005**, *15*, 925.
[46] S. Heun, R. F. Mahrt, A. Greiner, U. Lemmer, H. Bässler, D. A. Halliday, D. D. C. Bradley, P. L. Burn, A. B. Holmes, *J. Phys.: Condens. Matter* **1993**, *5*, 247–260.
[47] S. F. Alvarado, P. F. Seidler, D. G. Lidzey, D. D. C. Bradley, *Phys. Rev. Lett.* **1998**, *81*, 1082.
[48] R. Xia, M. Al-Hashimi, W.-C. Tsoi, M. Heeney, D. D. C. Bradley, J. Nelson, *Sol. Ener. Mater. Sol. Cells* **2012**, *96*, 112–116.
[49] C. R. Belton, A. L. Kanibolotsky, J. Kirkpatrick, C. Orofino, S. E. T. Elmasly, P. N. Stavrinou, P. J. Skabara, D. D. C. Bradley, *Adv. Funct. Mater.* **2013**, *23*, 2792–2804.
[50] H. Arwin, R. Jansson, *Electrochim. Acta* **1993**, *39*, 211.
[51] H. Z. T. Liu, S. Kwok, A. B. Djuriši , *J. Phys. D: Appl. Phys.* **2004**, *37*, 678–688.
[52] S. Adachi, *Optical Properties of Crystalline and Amorphous Semiconductors*, Kluwer Academic, New York, **1999**.
[53] A. R. Forouhi, I. Bloomer, *Phys. Rev. B* **1986**, *34*, 7018.
[54] M. Campoy-Quiles, J. Nelson, D. D. C. Bradley, P. G. Etchegoin, *Phys. Rev. B* **2007**, *76*, 235206.
[55] M. Campoy-Quiles, P. Etchegoin, D. D. C. Bradley, *Synth. Met.* **2005**, *155*, 279.
[56] P. Yu, M. Cardona, *Fundamentals of Semiconductors*, Springer-Verlag, Berlin, **1996**.
[57] M. Campoy-Quiles, T. Ferenczi, T. Agostinelli, P. G. Etchegoin, Y. Kim, T. D. Anthopoulos, P. N. Stavrinou, D. D. C. Bradley, J. Nelson, *Nat. Mater.* **2008**, *7*, 158–164.
[58] R. Osterbacka, C. P. An, X. M. Jiang, Z. V. Vardeny, *Science* **2000**, *287*, 839–842.
[59] U. Zhokhavets, R. Goldhahn, G. Gobsch, W. Schliefke, *Synth. Met.* **2003**, *138*, 491–495.
[60] M. Campoy-Quiles, Ph.D. Thesis, Imperial College London, **2005**.
[61] N. K. Persson, M. Sun, P. Kjellberg, T. Pullerits, O. Inganäs, *J. Chem. Phys.* **2005**, *123*, 204718.
[62] C. Ambrosch-Draxl, K. Hummer, S. Sagmeister, P. Puschnig, *Chem. Phys.* **2006**, *325*, 3–8.
[63] M. C. Gurau, D. M. DeLongchamp, B. M. Vogel, E. K. Lin, D. A. Fischer, S. Sambasivan, L. J. Richter, *Langmuir* **2007**, *23*, 834–842.
[64] A. J. Morfa, T. M. Barnes, A. J. Ferguson, D. H. Levi, G. Rumbles, K. L. Rowlen, J. van de Lagemaat, *J. Polym. Sci.Part B: Polym. Phys.* **2011**, *49*, 186–194.
[65] P. J. Brown, H. Sirringhaus, M. Harrison, M. Shkunov, R. H. Friend, *Phys. Rev. B* **2001**, *63*, 12.
[66] F. C. Spano, *J. Chem. Phys.* **2005**, *122*, 234701.
[67] J. Clark, J.-F. Chang, F. C. Spano, R. H. Friend, C. Silva, *Appl. Phys. Lett.* **2009**, *94*, 163306–163308.
[68] M. Grell, D. D. C. Bradley, M. Inbasekaran, E. P. Woo, *Adv. Mater.* **1997**, *9*, 798–802.
[69] M. Grell, M. Redecker, K. Whitehead, D. D. C. Bradley, M. Inbasekaran, E. P. Woo, *Liq. Cryst.* **1999**, *26*, 1403–1407.
[70] M. Grell, D. D. C. Bradley, *Adv. Mater.* **1999**, *11*, 895–905.
[71] K. S. Whitehead, M. Grell, D. D. C. Bradley, M. Jandke, P. Strohriegl, *Appl. Phys. Lett.* **2000**, *76*, 2946–2948.
[72] W. M. Prest, D. J. Luca, *J. Appl. Phys.* **1979**, *50*, 6067–6071.
[73] W. M. Prest, D. J. Luca, *J. Appl. Phys.* **1980**, *51*, 5170–5174.
[74] G. Leising, *Phys Rev. B* **1988**, *38*, 10313.

[75] J. Sturm, S. Tasch, A. Niko, G. Leising, E. Toussaere, J. Zyss, T. C. Kowalczyk, K. D. Singer, U. Scherf, J. Huber, *Thin Solid Films* **1997**, *298* 138.
[76] D. McBranch, I. H. Campbell, D. L. Smith, J. P. Ferraris, *Appl. Phys. Lett.* **1995**, *66*, 1175.
[77] E. K. Miller, M. D. McGehee, M. Diaz-Garcia, V. Srikant, A. J. Heeger, *Synth. Met.* **1999**, *102*, 1091–1092.
[78] C. M. Ramsdale, N. C. Greenham, *Adv. Mater.* **2002**, *14*, 212–215.
[79] M. Losurdo, G. Bruno, E. A. Irene, *J. Appl. Phys.* **2003**, *94*, 4923–4929.
[80] M. Tammer, R. W. T. Higgins, A. P. Monkman, *J. Appl. Phys.* **2002**, *91*, 4010.
[81] M. Campoy-Quiles, J. Nelson, P. G. Etchegoin, D. D. C. Bradley, U. Zhokhavets, G. Gobsch, H. Vaughan, A. Monkman, O. Inganäs, N. K. Persson, H. Arwin, M. Garriga, M. I. Alonso, G. Herrmann, M. Becker, W. Scholdei, M. Jahja, C. Bubeck, *Phys. Status Solidi C* **2008**, *5*, 1270–1273.
[82] S. Y. Chuang, H. L. Chen, W. H. Lee, Y. C. Huang, W. F. Su, W. M. Jen, C. W. Chen, *J. Mater. Chem.* **2009**, *19*, 5554–5560.
[83] H. Sirringhaus, P. J. Brown, R. H. Friend, M. M. Nielsen, K. Bechgaard, B. M. W. Langeveld-Voss, A. J. H. Spiering, R. A. J. Janssen, E. W. Meijer, P. Herwig, D. M. de Leeuw, *Nature* **1999**, *401*, 685–688.
[84] X. Zhang, L. J. Richter, D. M. DeLongchamp, R. J. Kline, M. R. Hammond, I. McCulloch, M. Heeney, R. S. Ashraf, J. N. Smith, T. D. Anthopoulos, B. Schroeder, Y. H. Geerts, D. A. Fischer, M. F. Toney, *J. Am. Chem. Soc.* **2011**, *133*, 15073–15084.
[85] J.-S. Kim, P. K. H. Ho, N. C. Greenham, R. H. Friend, *J. Appl. Phys.* **2000**, *88*, 1073–1081.
[86] T. Virgili, D. G. Lidzey, M. Grell, S. Walker, A. Asimakis, D. D. C. Bradley, *Chem. Phys. Lett.* **2001**, *341*, 219–224.
[87] G. Heliotis, R. Xia, K.S. Whitehead, G.A. Turnbull, I. D. W. Samuel, D.D.C. Bradley, *Synth. Met.* **2003**, *139*, 727–730.
[88] R. Xia, M. Campoy-Quiles, G. Heliotis, P. Stavrinou, K. S. Whitehead, D. D. C. Bradley, *Synth. Met.* **2005**, *155*, 274–278.
[89] H. Liem, P. Etchegoin, K. S. Whitehead, D. D. C. Bradley, *Adv. Funct. Mater.* **2003**, *13*, 66–72.
[90] M. C. Gather, D. D. C. Bradley, *Adv. Funct. Mater.* **2007**, *17*, 479–485.
[91] H. W. Lin, C. L. Lin, C. C. Wu, T. C. Chao, K. T. Wong, *Org. Electron.* **2007**, *8*, 189–197.
[92] O. P. Gaudin, I. D. W. Samuel, S. Amriou, P. L. Burn, *Appl. Phys. Lett.* **2010**, *96*, 053305.
[93] J. M. Winfield, C. L. Donley, J. S. Kim, *J. Appl. Phys.* **2007**, *102*, 063505.
[94] B. K. Yap, R. Xia, M. Campoy-Quiles, P. N. Stavrinou, D. D. C. Bradley, *Nat. Mater* **2008**, *7*, 376–380.
[95] M. Losurdo, M. M. Giangregorio, P. Capezzuto, G. Bruno, F. Babudri A. Cardone, C. Martinelli, G. M. Farinola, F. Naso, M. Büchel, *Polymer* **2008**, *49*, 4133–4140.
[96] Y. Kim, S. Cook, J. Kirkpatrick, J. Nelson, J. R. Durrant, D. D. C. Bradley, M. Giles, M. Heeney, R. Hamilton, I. McCulloch, *J. Phys. Chem. C* **2007**, *111*, 8137–8141.
[97] A. Boudrioua, P. A. Hobson, B. Matterson, I. D. W. Samuel, W. L. Barnes, *Synth. Met.* **2000**, *111*, 545–547.
[98] W. A. McGahan, B. Johs, J. A. Woollam, *Thin Solid Films* **1993**, *234*, 443.
[99] O. Levy, D. Stroud, *Phys Rev B* **1997**, *56*, 8035.
[100] S. Giordano, *J. Electrost.* **2006**, *64*, 655–663.
[101] B. O'Connor, R. J. Kline, B. R. Conrad, L. J. Richter, D. Gundlach, M. F. Toney, D. M. DeLongchanp, *Adv. Funct. Mater.* **2011**, *21*, 3697–3705.
[102] D. M. DeLongchamp, R. J. Kline, E. K. Lin, D. A. Fischer, L. J. Richter, L. A. Lucas, M. Heeney, I. McCulloch, J. E. Northrup, *Adv. Mater.* **2007**, *19*, 833–837.
[103] U. Zhokhavets, T. Erb, G. Gobsch, M. Al-Ibrahim, O. Ambacher, *Chem. Phys. Lett.* **2006**, *418*, 347.
[104] M. Sims, S. M. Tuladhar, J. Nelson, R.C. Maher, M. Campoy-Quiles, S. A. Choulis, M. Mairy, D. D. C. Bradley, P. G. Etchegoin, C. Tregidgo, K. Suhling, D. R. Richards, P. Massiot, C. B. Nielsen, J. H. G. Steinke, *Phys. Rev. B* **2007**, *76*, 195206.
[105] M. Grell, D. D. C. Bradley, X. Long, T. Chamberlain, M. Inbasekaran, E. P. Woo, M. Soliman, *Acta Polymer.* **1998**, *49*, 439–444.
[106] M. Grell, D. D. C. Bradley, *Adv. Mater.* **1999**, *11*, 895–905.
[107] T. Kreouzis, D. Poplavskyy, S. M. Tuladhar, M. Campoy-Quiles, J. Nelson, A. J. Campbell, D. D. C. Bradley, *Phys. Rev. B* **2006**, *73*, 235201.
[108] P. N. Stavrinou, G. Ryu, M. Campoy-Quiles, D. D. C. Bradley, *J. Phys. Condens. Matter* **2007**, *19*, 466107.
[109] D. Nassyrov, C. Müller, A. Roigé, I. Burgués-Ceballos, O. J. Ossó, D. B. Amabilino, M. Garriga, M. I. Alonso, A. R. Goñi, M. Campoy-Quiles, *J. Mater. Chem.*, **2012**, *22*, 4519–4526.
[110] I. Burgués-Ceballos, M. Campoy-Quiles, L. Francesch, P. D. Lacharmoise, *J. Polym. Scien. Part B: Poly. Phys.*, **2012**, *50*, 1245–1252.
[111] M. R. Hammond, R. J. Kline, A. A. Herzing, L. J. Richter, D. S. Germack, H.-W. Ro, C. L. Soles, D. A. Fischer, T. Xu, L. Yu, M. F. Toney, D. M. DeLongchamp, *ACS Nano* **2011**, *5*, 8248–8257.
[112] N. K. Patel, S. Cina, J. H. Burroughes, *IEEE J Sel Top Quant Elec* **2002**, *8*, 346.
[113] L. Chen, P. Degenaar, D.D.C. Bradley, *Adv. Mater.* **2008**, *20*, 1679–1683.
[114] T. Ameri, G. Dennler, C. Lungenschmied, C. J. Brabec, *Energy Environ Sci* **2009**, *2*, 347–363.
[115] L. A. A. Pettersson, L. S. Roman, O. Inganäs, *J. Appl. Phys.* **1999**, *86*, 487–496.
[116] J. Gilot, I. Barbu, M. M. Wienk, R. A. J. Janssen, *Appl. Phys. Lett.* **2007**, *91*, 11350.
[117] R. Hausermann, E. Knapp, M. Moos, N. A. Reinke, T. Flatz, *J. Appl. Phys.* **2009**, *106*, 104507.
[118] O. E. Semonin, J. M. Luther, S. Choi, H.-Y. Chen, J. Gao, A. J. Nozik, M. C. Beard, *Science* **2011**, *334*, 1530.
[119] G. F. Burkhard, E. T. Hoke, S. R. Scully, M. D. McGeHee, *Nano Lett.* **2009**, *9*, 4037–4041.
[120] L.-M. Chen, A. Hong, G. Li, Y. Yang, *Adv. Mater.* **2009**, *27*, 1–16.
[121] M. Sims, K. Zheng, M. Campoy-Quiles, R. Xia, D. D. C. Bradley, P. Etchegoin, *J. Phys.: Condens. Matter* **2005**, *17*, 1–12.
[122] a) D. A. G. Bruggeman, *Ann. Phys. Leipzig* **1935**, *24*, 636; b) T. C. Choy, *Effective Medium Theory: Principles and Applications*, Oxford University Press, Oxford, **1999**.
[123] J. Koh, Y. Lu, C. R. Wronski, Y. Kuang, R. W. Collins, T. T. Tsong, Y. E. Strausser, *Appl. Phys. Lett.* **1996**, *69*, 1297–1299.
[124] P. Petrik, L. P Biró, M. Fried, T. Lohner, R. Berger, C. Schneider, J. Gyulai, H. Ryssel, *Thin Solid Films* **1998**, *315*, 186–191.
[125] D. E. Markov, J. C. Hummelen, P. W. M. Blom, A. B. Sieval, *Phys. Rev. B* **2005**, *72*, 045216.
[126] C. W. Rochester, S. A. Mauger, A. J. Moule, *J Phys Chem C* **2012**, *116*, 7287–7297.
[127] T. A. M. Ferenczi, J. Nelson, C. Belton, A. M. Ballantyne, M. Campoy-Quiles, F. M. Braun, D. D. C. Bradley, *J. Phys.: Condens. Matter* **2008**, *20*, 475203.
[128] M. Campoy-Quiles, C. Müller, M. Garriga, E. Wang, O. Inganäs, M. I. Alonso, *Thin Solid Films* **2013**, unpublished.
[129] U. Zhokhavets, R. Goldhahn, G. Gobsch, M. Al-Ibrahim, H. K. Roth, S. Sensfuss, E. Klemm, D. A. M. Egbe, *Thin Solid Films* **2003**, *444*, 215–220.
[130] K. Vandewal, K. Tvingstedt, A. Gadisa, O. Inganäs, J. V. Manca, *Nat. Mater.* **2009**, *8*, 904.
[131] C. Müller, J. Bergqvist, K. Vandewal, K. Tvingstedt, A. S. Anselmo, R. Magnusson, M. I. Alonso, E. Moons, H. Arwin, M. Campoy-Quiles, O. Inganäs, *J. Mater. Chem.* **2011**, *21*, 10676–10684.

[132] S. Engmann, V. Turkovic, G. Gobsch, H. Hoppe, *Adv. Ener. Mater.* **2011**, *1*, 684.
[133] S. Engmann, V. Turkovic, P. Denner, H. Hoppe, G. Gobsch, *J. Pol. Scien. Pol. Phys.* **2012**, *50*, 1363.
[134] D. S. Germack, C. K. Chan, R. J. Kline, D. A. Fischer, D. J. Gundlach, M. F. Toney, L. J. Richter, D. M. DeLongchamp, *Macromolecules* **2010**, *43*, 3828–3836.
[135] T. Agostinelli, S. Lilliu, J. G. Labram, M. Campoy-Quiles, M. Hampton, E. Pires, J. Rawle, O. Bikondoa, D. D. C. Bradley, T. D. Anthopoulos, J. Nelson, J. E. Macdonald, *Adv. Funct. Mater.* **2011**, *21*, 1701–1708.
[136] A. Guerrero, B. Dörling, T. Ripolles-Sanchis, M. Aghamohammadi, E. Barrena, M. Campoy-Quiles, G. Garcia-Belmonte, *ACS Nano* **20 13**, *7*, 4637–4646.
[137] M. Campoy-Quiles, V. Randon, M. M. Mróz, M. Jarzaguet, M. Garriga, J. Cabanillas-Gonzalez, *Org. Photonics Photovoltaics* **2013**, *1*, 11–23.
[138] J. W. Kiel, B. J. Kirby, C. F. Majkrzak, B. B. Maranvile, M. E. MacKay, *Soft Mater* **2010**, *6*, 641–646.
[139] A. J. Parnell, A. D. F. Dunbar, A. J. Pearson, P. A. Staniec, A. J. C. Dennison, H. Hamamatsu, M. W. A. Skoda, D. G. Lidzey, R. A. L. Jones, *Adv. Mater.* **2010**, *22*, 2444–2447.
[140] T. Ino, T. Hayashi, T. Fukuda, K. Ueno, H. Shirai, *Phys. Status Solidi C* **2011**, *8*, 2973–3029.
[141] M. Grell, D. D. C. Bradley, M. Inbasekaran, E. P. Woo, *Adv. Mater.* **1997**, *9*, 798–802.
[142] J. M. G. Cowie, *Polymers: Chemistry and Physics of modern materials*, 2nd Ed., Blackie Academic and Professional **1996**.
[143] J. L. Keddie, R. A. L. Jones, R. A. Cory, *Europhys. Lett.* **1994**, *27*, 59.
[144] J. H. Kim, J. Jang, W. Zin, *Langmuir* **2000**, *16*, 4064.
[145] Y. Grohens, M. Brogly, C. Labbe, M. D. David, J. Schultz, *Langmuir* **1998**, *14*, 2929.
[146] L. Singh, P. J. Ludovice, C. L. Henderson, *Thin Solid Films* **2004**, *449*, 231.
[147] D. M. Delongchamp, R. J. Kline, Y. Jung, E. K. Lin, D. A. Fischer, D. J. Gundlach, S. K. Cotts, A. J. Moad, L. J. Richter, M. F. Toney, M. Heeney, I. McCulloch, *Macromolecules* **2008**, *41*, 5709–5715.
[148] C. J. Ellison, J. M. Torkelson, *Nat. Mater.* **2003**, *2*, 695.
[149] S. Sills, R. M. Overney, W. Chau, V. Y. Lee, R. D. Miller, J. Frommer, *J. Chem. Phys.* **2004**, *120*, 5334.
[150] A. Roigé, M. Campoy-Quiles, J. O. Ossó, M. I. Alonso, L. F. Vega, M. Garriga, *Synth. Met.* **2012**, *161*, 2570.
[151] C. Müller, L. M. Andersson, O. Peña-Rodríguez, M. Garriga, O. Inganäs, M. Campoy-Quiles, *Macromolecules* **2013**, *46*, 7325–7331.
[152] C. Müller, T. A. M. Ferenczi, M. Campoy-Quiles, J. M. Frost, D. D. C. Bradley, P. Smith, N. Stingelin-Stutzmann, J. Nelson, *Adv. Mater.* **2008**, *20*, 3510–3515.
[153] T. Wang, A. J. Pearson, D. G. Lidzey, R. A. L. Jones, *Adv. Funct. Mater.* **2011**, *21*, 1383–1390.
[154] B. Schmidt-Hansberg, M. F. G. Klein, K. Peters, F. Buss, J. Pfeifer, S. Walheim, A. Colsmann, U. Lemmer, P. Scharfer, W. Schabe, *J. Appl. Phys.* **2009**, *106*, 124501.
[155] S. Y. Heriot, R. A. L. Jones, *Nat. Mater.* **2005**, *4*, 782–786.
[156] U. Heinemeyer, K. Broch, A. Hinderhofer, M. Kytka, R. Scholz, A. Gerlach, F. Schreiber, *Phys. Rev. Lett.* **2010**, *104*, 257401.